Experimental Multipartite Entanglement Detection With Minimal-Size Correlations

Dian Wu,[1,2,*] Fei Shi,[3,†] Jia-Cheng Sun,[1] Bo-Wen Wang,[1]
Xue-Mei Gu,[4] Giulio Chiribella,[3,5,6,‡] Qi Zhao,[3,§] and Jian Wu[1,7,8]

[1]*Advanced Institute of Precision Spectroscopy, East China Normal University, Shanghai 200241, China*
[2]*Shanghai Branch, Hefei National Laboratory, Shanghai 201315, China*
[3]*QICI Quantum Information and Computation Initiative, School of Computing and Data Science, The University of Hong Kong, Pokfulam Road, Hong Kong SAR, China*
[4]*Institut für Festkörpertheorie und Optik, Friedrich-Schiller-Universität Jena, Max-Wien-Platz 1, 07743 Jena, Germany*
[5]*Department of Computer Science, Parks Road, Oxford, OX1 3QD, United Kingdom*
[6]*Perimeter Institute for Theoretical Physics, Waterloo, Ontario N2L 2Y5, Canada*
[7]*Chongqing Key Laboratory of Precision Optics, Chongqing Institute of East China Normal University, Chongqing 401121, China*
[8]*Collaborative Innovation Center of Extreme Optics, Shanxi University, Taiyuan, Shanxi 030006, China*

Multiparticle entanglement is a valuable resource for quantum technologies, including measurement based quantum computing, quantum secret sharing, and a variety of quantum sensing applications. The direct way to detect this resource is to observe correlations arising from local measurements performed simultaneously on all particles. However, this approach is increasingly vulnerable to measurement imperfections when the number of particles grows, and becomes unfeasible for large-scale entangled states. It is therefore crucial to devise detection methods that minimize the number of simultaneously measured particles. Here we provide the first experimental demonstration of multipartite entanglement detection with minimal-size correlations, showing that our setup is robust to misalignment of the local measurement bases and enables the certification of genuine multipartite entanglement in a regime where the direct approach fails. Overall, our results indicate a promising route to the experimental detection of genuine multipartite entanglement in large-scale entangled states.

Introduction.— Entanglement is one of the cornerstones of quantum information science, and is as one of the key resources in quantum computation [1–3], communication [4–6], and metrology [7–9]. With the advancement of quantum technologies, the size and complexity of the entangled states accessible in the laboratory is rapidly increasing; for example, globally entangled states of 51-qubit and 95-qubit have been recently generated in superconducting qubit systems [10, 11].

As the size of the accessible entangled states scales up, certifying the presence of genuine multipartite entanglement (GME)—the strongest form of nonclassical correlation—becomes increasingly important. This task, however, presents major challenges. The direct approach to GME detection requires either performing global measurements (*e.g.,* measurements on a basis that include the entangled state of interest) or estimating correlations among local measurements performed simultaneously on all particles [12–19]. When the number of particles becomes large, however, this approach becomes problematic: on the one hand, large-scale entangled measurements are hard to implement, and on the other hand correlations among a large number of particles are very sensitive to experimental imperfections. For example, it has been found that small deviations between the single-particle measurements required by the theory and the measurements actually performed in the laboratory can result in a high rate of false positives [20–23]. Therefore, it is essential to reduce the number of particles and to develop detection methods that involve only a small number of particles.

Over the past two decades, significant efforts have been devoted to detection methods that require measurements on fewer particles [13, 24–31], and to the study of related problems, such as the entanglement marginal problem [32] and the entanglement transitivity problem [33]. Very recently, Ref. [34] introduced the notion of *entanglement detection length (EDL)*, defined as the minimum number of particles that must be simultaneously measured in order to detect genuine multipartite entanglement. The EDL sets the ultimate in-principle limit to the size of the correlations required for entanglement detection, and provides useful guidance in designing robust, scalable detection schemes using only few-particle observables. However, no systematic experimental demonstrations of entanglement detection have reached the EDL limit.

In this letter, we present a proof-of-concept demonstration of entanglement detection at the EDL limit. Using a photonic platform, we detect the multipartite entanglement of states in three important classes: W states, Dicke states, and cluster states. Our experiment includes a high-fidelity preparation of prepare three- and four-qubit states and the verification of their GME by performing few-particle measurements at the EDL limit. For the

* dwu@lps.ecnu.edu.cn; These two authors contributed equally to this work.
† shifei@hku.hk; These two authors contributed equally to this work.
‡ giulio@cs.hku.hk
§ zhaoqi@cs.hku.hk

four-qubit Dicke state, we show that the EDL witness is more robust to measurement errors than the projector witness that relies on global measurements, representing the first experimental demonstration of the advantage of EDL-sized measurements for entanglement detection.

EDL witnesses.—A density matrix of n-particles is called *biseparable* if it is a convex combination of separable states over different bipartitions, and is called *genuinely entangled* if it is not biseparable [35]. In the following, we will label the n particles by integers from 1 to n, and we will represent subsystems of the n-particle system by subsets of the set $\{1, \ldots, n\}$. For a genuinely entangled state ρ, we say that a collection of subsets $\mathcal{S} := \{S_1, \ldots, S_t\}$ *detect ρ's GME* if the GME of the state ρ can be certified by performing measurements on the subsystems corresponding to the subsets in $\mathcal{S}$ [34].

For a collection of subsets that detect ρ's GME, an important question is how many particles are contained in each subset, that is, how many particles have to be jointly measured in order to detect ρ's GME. The minimum such number is called the *EDL of the state* ρ [34], and will hereafter be denoted by $l(\rho)$. An illustration of the notion of EDL in a few special cases is provided in Fig. 1.

By definition, any experimental scheme for detecting the GME of the state ρ must involve at least one k-particle measurement with $k \geq l(\rho)$. Since measurements on larger numbers of particles are generally more sensitive to noise, it is important to design entanglement detection schemes that reach the EDL limit, that is, entanglement detection schemes using measurements on exactly $l(\rho)$ particles.

To enable detection of GME at the EDL limit, we use a suitable variant of the method of entanglement witnesses [35]. An n-particle observable W is a witness for ρ's GME if $\mathcal{W}$ has nonnegative expectation values for all biseparable states, and a negative expectation value on ρ. Using semidefinite programming (SDP), we show that, if a collection of subsets $\mathcal{S}$ detects ρ's GME, then it is possible to construct a witness $\mathcal{W}$ of ρ's GME and is supported on $\mathcal{S}$ (see End Matter), that is, a witness of the form $\mathcal{W} := \sum_{S \in \mathcal{S}} B_S \otimes \mathbb{I}_{S^c}$, where B_S is a Hermitian operator on the Hilbert space associated to particles in the set S, and $\mathbb{I}_{S^c}$ is an identity operator on the Hilbert space associated to particles in the complementary set $S^c := \{1, \ldots, n\} \setminus S$. Then, we define an *EDL witness* as a witness associated to a collection of EDL-sized subsets $\mathcal{S}$, that is, a collection $\mathcal{S}$ such that $|S| = l(\rho)$ for every subset $S \in \mathcal{S}$.

We now provide EDL witnesses for four paradigmatic examples of states: W states of 3 and 4 qubits, 4-qubit

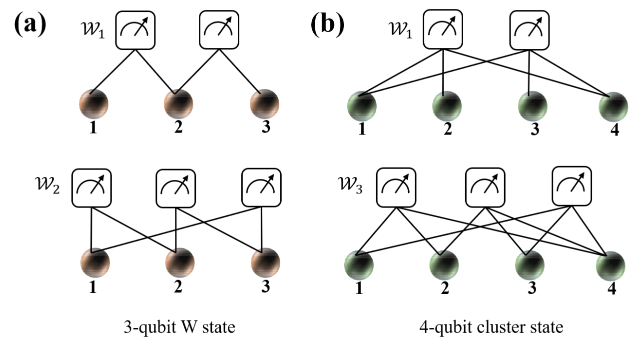

FIG. 1. Entanglement detection length (EDL) is the minimum number of parties that must be jointly measured to certify a state's genuine multipartite entanglement (GME). For example, the EDL for a W state is 2, whereas the EDL for a cluster state is 3. (a) For the 3-qubit W state, we consider two EDL witnesses, $\mathcal{W}_1$ and $\mathcal{W}_2$, constructed from two-body joint measurements over the pairs $\{12, 23\}$ and $\{12, 23, 13\}$, respectively. (b) For the 4-qubit cluster state, we consider two EDL witnesses, $\mathcal{W}_1$ and $\mathcal{W}_3$, constructed from three-body joint measurements over the triplets $\{124, 134\}$ and $\{124, 234, 134\}$, respectively.

Dicke state, and 4-qubit cluster state, explicitly given by

$$\begin{aligned}
|\mathrm{W}_3\rangle &= (|001\rangle + |010\rangle + |100\rangle)/\sqrt{3}, \\
|\mathrm{W}_4\rangle &= (|0001\rangle + |0010\rangle + |0100\rangle + |1000\rangle)/2, \\
|\mathrm{D}_4\rangle &= (|0011\rangle + |0101\rangle + |0110\rangle \\
&\quad + |1001\rangle + |1010\rangle + |1100\rangle)/\sqrt{6}, \\
|\mathrm{C}_4\rangle &= (|0000\rangle + |0011\rangle + |1100\rangle - |1111\rangle)/2.
\end{aligned} \tag{1}$$

The EDL of these states is $l(|\mathrm{W}_3\rangle) = l(|\mathrm{W}_4\rangle) = l(|\mathrm{D}_4\rangle) = 2$, and $l(|\mathrm{C}_4\rangle) = 3$, respectively [34], and EDL witnesses using only 2-particle and 3-particle correlations are constructed in the End Matter (see also Table II for a quick summary.)

We now analyze the robustness of EDL witnesses to noise and measurement imperfections. In general, entanglement witnesses are robust to small amounts of white noise. If an n-qubit state ρ can be detected by the witness $\mathcal{W}$, then its noisy version $\rho(p) = (1-p)\rho + p(\mathbb{I}/2^n)$ can be also detected by $\mathcal{W}$, provided that the amount of white noise p is below the maximum value $p_{\text{noise}} := \mathrm{Tr}(\mathcal{W}\rho)/[\mathrm{Tr}(\mathcal{W}\rho) - \mathrm{Tr}(\mathcal{W})/2^n]$. For example, let us consider two witnesses for the 4-qubit Dicke state. The first witness is an EDL witness based on the collection of subsets $\{12, 23, 34, 14, 13, 24\}$. This witness, denoted by $\mathcal{W}_5$ in the End Matter, has noise robustness $p_{\text{noise}} = 0.3131$. The second witness is the projector witness, $\mathcal{W}_{\text{proj}} = (2/3)\mathbb{I} - |\mathrm{D}_4\rangle\langle\mathrm{D}_4|$, which requires measurements on all qubits and has noise robustness $p_{\text{noise}} = 0.3556$ [36]. While the projector witness appears to have higher robustness than the EDL witness, it is important to note that the robustness was defined under the assumption that the setup in the laboratory performs exactly the right measurements appearing in the decomposition of the witness. We now show that, in the presence of measurement imperfections, the EDL witness can offer higher

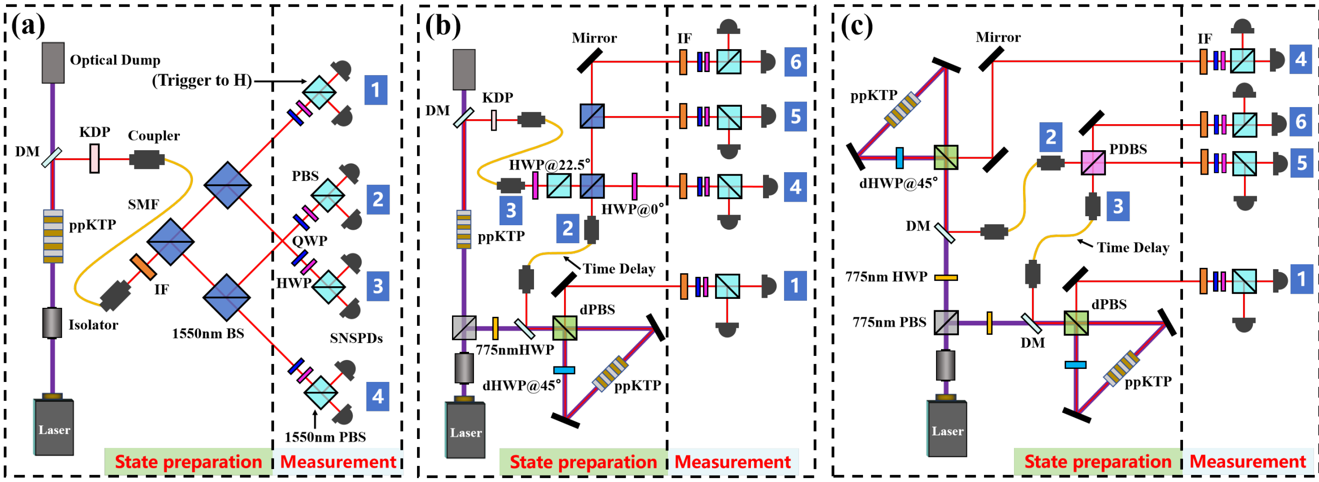

FIG. 2. Experimental setup. A mode-locked Ti:sapphire laser (775 nm, 80 MHz) pumps a periodically poled $KTiOPO_4$ (ppKTP) crystal, producing photon pairs via type-II spontaneous parametric down-conversion (SPDC). An optical isolator directly after the laser suppresses back-reflections. Residual pump light is removed with a dichroic mirror (DM), and temporal walk-off is compensated using a potassium dihydrogen phosphate (KDP) crystal. After spectral filtering with interference filters (IFs), two-photon interference is implemented on beam-splitter / polarization-dependent beam-splitter (BS/PDBS) networks; the interphoton delay is tuned by a motorized translation stage to ensure temporal overlap. Each output mode is analyzed by a standard quarter-wave-plate–half-wave-plate–polarizing-beam-splitter (QWP–HWP–PBS) module implementing the required local projective settings. Photons are coupled into single-mode fibers (SMFs) and detected with superconducting nanowire single-photon detectors (SNSPDs, $\approx 90\%$ efficiency); fourfold coincidences are recorded with a multichannel coincidence counter. Here, dHWP and dPBS denote a dual-wavelength half-wave plate (775/1550 nm) and a dual-wavelength polarizing beam splitter (775/1550 nm), respectively. (a) Four-photon Dicke and heralded three-photon W states. (b) Four-photon W states. (c) Four-photon cluster states.

robustness. For instance, assume that the measurement bases for each particle are misaligned as follows:

$$
\begin{aligned}
X &\to X(\theta) = \cos(\theta)X + \sin(\theta)Y, \\
Y &\to Y(\theta) = \cos(\theta)Y + \sin(\theta)Z, \\
Z &\to Z(\theta) = \cos(\theta)Z + \sin(\theta)X,
\end{aligned}
\tag{2}
$$

we compare the white noise tolerances p_{noise} of these two witnesses in Fig. 3(a). When $\theta > 0.26$, the EDL witness exhibits greater white noise tolerances than the projector witness. Notably, this advantage of the EDL witness persists even when the misalignment angle is introduced solely on Y, as shown in Fig. 3(b).

It is also interesting to anlyze different EDL witnesses for the same state, and to observe how the noise robustness depends on the subsets of measured particles. In the cases under consideration, we find that increasing the number of subsets typically increases the robustness. For example, we compare two witnesses $\mathcal{W}_1$ and $\mathcal{W}_2$ for the three-qubit W state. $\mathcal{W}_1$ uses measurements on the subsets $\{1,2\}$ and $\{2,3\}$, and tolerates $p_{\text{noise}} = 0.1859$ noise, whereas $\mathcal{W}_2$ uses measurements on all 2-qubit subsets and tolerates a higher level of noise $p_{\text{noise}} = 0.3039$. It is also worth mentioning that another witness for the 3-qubit W state was previously known [13]. This witness is also an EDL witness, as it uses measurements on all two-qubits subsets. Compared to the witness $\mathcal{W}_2$ constructed here, it appears to have less noise tolerance ($p_{\text{noise}} = 0.19$.)

Experimental realization.— Our experimental setup for the demonstration of entanglement detection at the EDL limit is depicted in Fig.2(a), four spatially indistinguishable photons in the polarization state $|HVHV\rangle$, with H and V denoting horizontal and vertical polarizations encoding logical 0 and 1, are generated via second-order emission in collinear type-II SPDC. The photons are then distributed into four spatial modes using three 50:50 beam splitters (BSs). Detection of one photon in each mode indicates the successful preparation of the four-photon Dicke state defined in Eq.(1) [37]. In Fig. 3, we compare our setup with the global measurement method commonly used in entanglement detection experiments [38–41], showing that the EDL offers increased robustness to imperfection in the choice of measurement bases.

Using a standard fidelity-measurement protocol [36], we prepare four-photon Dicke states with fidelities of 0.925(3), 0.894(3), and 0.849(3). To emulate calibration drifts that differ across settings, we applied Eq. (2) with a fixed magnitude $\theta = 2\pi/15, \pi/8$ and $\pi/9$ to construct *per-setting* offset axes $X(\theta), Y(\theta), Z(\theta)$. The same three offset measurement directions were used identically at all four measurement stations to evaluate both the global projector/fidelity witness and the EDL witnesses. Under these conditions, the fidelity drop to 0.611(4), 0.603(4) and 0.645(4), giving $\mathcal{W}_{\text{proj}}(2\pi/15) = 0.056(4) > 0, \mathcal{W}_{\text{proj}}(\pi/8) = 0.064(4) > 0, \mathcal{W}_{\text{proj}}(\pi/9) = 0.022(4) > 0$ and thus no certification of GME, whereas the EDL witness yield $\mathcal{W}_5(2\pi/15) = -0.0029(6) < 0, \mathcal{W}_5(\pi/8) = -0.0037(6) < 0, \mathcal{W}_5(\pi/9) = -0.0063(6) < 0$, certifying GME. A comparison of the expectation values is shown in Fig. 3(c). Then, we prepare four-photon Dicke

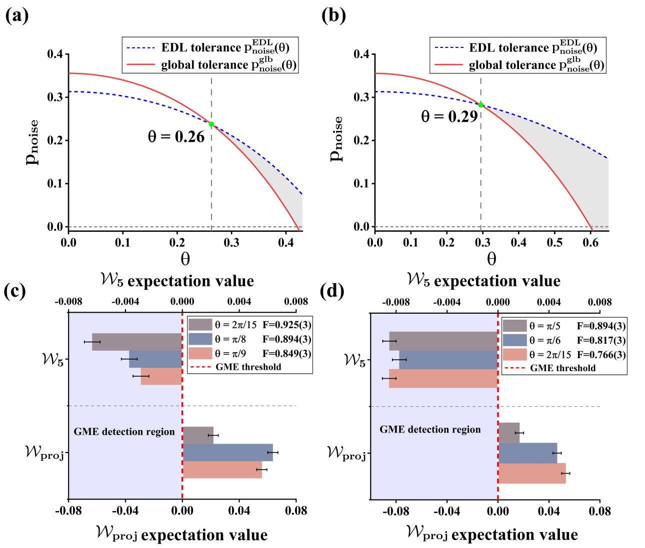

FIG. 3. Theoretical predictions of white noise tolerance and experimental comparison results. (a) White noise tolerances of the EDL witness and the projector/global witness versus measurement bases misalignment θ. When $\theta > 0.26$, the EDL witness exhibits greater white noise tolerances than the projector witness. (b) White noise tolerances when the misalignment θ is only introduced on the basis Y. When $\theta > 0.29$, the EDL witness exhibits greater white noise tolerances than the projector witness. (c) Experimental results of measurement-noise robustness for the four-photon Dicke state: comparison between the global-measure (fidelity) witness $\mathcal{W}_{\rm proj}$ and the EDL two-body witness W_5 (designed for $p_{\rm noise} = 0.313$), evaluated under the global measure with measurement bases misalignment $\theta = 2\pi/15$, $\theta = \pi/8$, and $\theta = \pi/9$. (d) Comparison results of measurement noise introduced only on the basis Y with measurement bases misalignment$\theta = \pi/5$, $\theta = \pi/6$, and $\theta = 2\pi/15$ at all four measurement stations. Error bars indicate one standard deviation obtained by propagating Poissonian counting statistics of the raw counts.

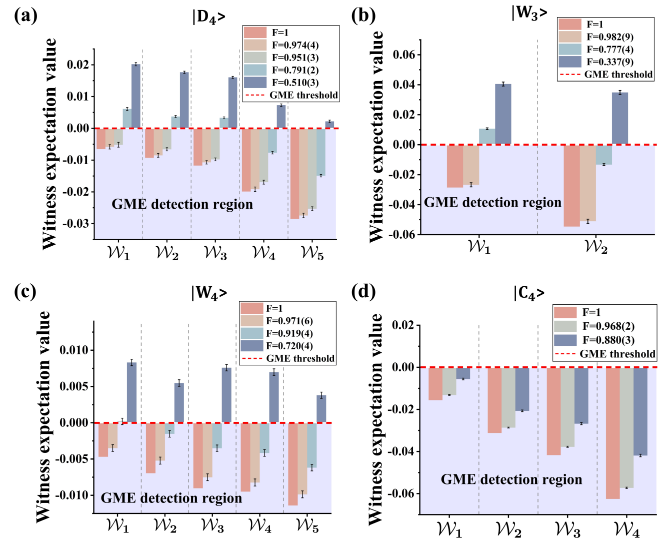

FIG. 4. Experimental results. (a) Four-photon Dicke states; (b) three-photon W states; (c) four-photon W states; (d) four-photon cluster states. Bars show measured witness values, with bar colors denoting the experimentally prepared entangled-state fidelities; an ideal $F = 1$ reference is included for comparison. The red dashed zero line marks the GME threshold (negative values certify genuine multipartite entanglement). EDL-constructed witnesses $\mathcal{W}_i$ are shown together with their predicted maximum tolerable white-noise fractions p_i. Error bars indicate one standard deviation obtained by propagating Poissonian counting statistics of the raw counts.

state with fidelity 0.817(3), 0.894(3) and 0.766(3) to perform $\theta = \pi/5, \pi/6$ and $2\pi/15$ only on basis $Y(\theta)$ at all four measurement stations. The experimental results still demonstrate the robustness advantage of the EDL method as shown in Fig. 3(d).

In addition, we verify the correctness of the witness' predictions within its noise range and at the noise boundary under various noise coefficients. By tuning the experimental parameters, we prepare $|\mathrm{D}_4\rangle$ states with fidelities of 0.974(4), 0.951(3), 0.791(2), and 0.510(3)(see Appendix), corresponding to different $p_{\rm noise}$. This set spans a wide range of noise, allowing a systematic assessment of the robustness of the EDL witnesses and a quantitative comparison between theory and experiment. The corresponding results are shown in Fig. 4(a).

For W states, we prepare states of both 3-qubit and 4-qubit systems. Using the setup in Fig.2(a), we generate a four-photon Dicke state and herald an $|H\rangle$ photon in mode 1 to prepare the three-photon W state. To benchmark the noise resilience of EDL witnesses, we prepare $|\mathrm{W}_3\rangle$ with three distinct fidelities—0.982(9), 0.777(4), and 0.337(9) (see Appendix). The two EDL witnesses remain robustly negative across this range, as shown in Fig.4(b).

As shown in Fig.2(b), a pulsed laser is split by a polarizing beam splitter into two paths, generating photon pairs in the states $|HV\rangle$ and $(|HV\rangle + |VH\rangle)/\sqrt{2}$ via SPDC. To ensure temporal overlap of photons in spatial modes 2 and 3 at the beam splitter, a motorized translation stage is used to adjust their relative delay. A Hong–Ou–Mandel interference measurement yields a visibility of 0.989(2) (see Appendix), confirming near-ideal indistinguishability. A four-photon W state is prepared by detecting one photon in mode 1 and one in each of modes 4, 5, and 6 after the beam splitter [42]. The EDL framework provides five EDL witnesses with distinct noise tolerances for the four-photon $|\mathrm{W}_4\rangle$ state. We prepare $|\mathrm{W}_4\rangle$ states with fidelities of 0.971(6), 0.919(4), and 0.720(4), and test each witness accordingly (see Appendix). As expected from theory, the measurements in Fig.4(c) confirm that the state of fidelity 0.919(4) is detected by $\mathcal{W}_2$ ($p_{\rm noise} = 0.100$) but fails to be detected by $\mathcal{W}_1$ ($p_{\rm noise} = 0.070$).

Within the EDL framework, the EDL for a W state or a Dicke state is 2, whereas the EDL for a cluster state is 3. Guided by this structure, we experimentally implement four EDL witnesses to detect GME in a four-photon cluster state $|\mathrm{C}_4\rangle$. According to the Fig.2(c), a pulsed laser pumps the ppKTP crystal in a Sagnac loop, generating two entangled photon pairs $|\psi\rangle = \frac{1}{2}|HH\rangle + \frac{\sqrt{3}}{2}|VV\rangle$

through SPDC. Photons in spatial modes 2 and 3 interfere at a PDBS characterized by transmittance $T_V = \frac{1}{3}$, $R_V = \frac{2}{3}$, $T_H = 1$, and $R_H = 0$. A four-photon cluster state [43] is obtained by detecting one photon in each of output modes 5 and 6, along with one photon in each of local modes 1 and 4. Experimental implementations under two distinct conditions (detailed in Appendix), achieving $|\mathrm{C}_4\rangle$ with fidelities of 0.968(2) and 0.880(3). The corresponding experimental results are presented in Fig.4(d).

Conclusions.— We reported the first experimental demonstration of the entanglement detection length framework for certifying genuine multipartite entanglement. By preparing a photonic multipartite states with varied configurations and fidelities, we showed that EDL witnesses can achieve accurate certification using only few-body observables supported on the minimum number of particles. Compared with conventional global-projector methods, the EDL approach appears to have increased robustness to measurement imperfections, as measuring less particles generally reduces the impact of basis misalignment. These results constitute a proof-of-principle that EDL provides a scalable, tomography-free, and noise-robust route to the verification of multipartite entanglement.

Acknowledgments. This work was supported by the Chinese Ministry of Science and Technology (MOST) through grant 2023ZD0300600, by the National Natural Science Foundation of China under the General Program, Grant No. 12474487, Shanghai Pilot Program for Basic Research (TQ20240204), and the Science and Technology Commission of Shanghai Municipality (231c1402900). FS and QZ acknowledge funding from Innovation Program for Quantum Science and Technology via Project 2024ZD0301900, National Natural Science Foundation of China (NSFC) via Project No. 12347104 and No. 12305030, Guangdong Basic and Applied Basic Research Foundation via Project 2023A1515012185, Hong Kong Research Grant Council (RGC) via No. 27300823, N_HKU718/23, and R6010-23, Guangdong Provincial Quantum Science Strategic Initiative No. GDZX2303007, HKU Seed Fund for Basic Research for New Staff via Project 2201100596. GC acknowledges Hong Kong Research Grant Council (RGC) through grants SRFS2021-7S02 and R7035-21F, and the State Key Laboratory of Quantum Information Technologies and Materials.

End Matter

The construction of witnesses using measurement supported on a collection of subsets $\mathcal{S}$ can be formulated as the following semidefinite program (SDP) [34, 54]; specifically, the SDP for a given entangled state ρ is

$$
\begin{aligned}
&\alpha(\rho,\mathcal{S}) := \min \mathrm{Tr}(\mathcal{W}\rho),\\
&\text{s.t.}\quad \mathrm{Tr}(\mathcal{W}) = 1,\\
&\mathcal{W} = \sum_{S\in\mathcal{S}} B_S \otimes \mathbb{I}_{S^c},\\
&\text{for all bipartitions } A|A^c,\\
&\mathcal{W} = P_A + Q_A^{T_A},\quad P_A \geq 0,\quad Q_A \geq 0,
\end{aligned} \tag{3}
$$

where, for every subset S, B_S is a Hermitian operator on $\mathcal{H}_S := \bigotimes_{i\in S}\mathcal{H}_i$, and $\mathbb{I}_{S^c}$ is an identity operator on $\mathcal{H}_{S^c}$, T_A is the partial transpose with respect to A. If $\alpha(\rho,\mathcal{S}) < 0$, then $\mathcal{S}$ detects ρ's GME, and the witness is $\mathcal{W}$, with $p_{\text{noise}} = 2^n\alpha(\rho,\mathcal{S})/[2^n\alpha(\rho,\mathcal{S}) - 1]$.

By using the above SDP, we can construct several EDL witnesses for the 3,4-qubit W states, the 4-qubit Dicke state, and the 4-qubit cluster state. Note that for the EDL witness of 3-qubit W state, $Z_1 := Z\otimes I\otimes I$, $X_1X_2 := X\otimes X\otimes I$, $Y_1Y_3 := Y\otimes I\otimes Y$, etc, where X, Y, Z, I are the Pauli matrices.

EDL witnesses for the 3-qubit W state:

1) $\mathcal{S}_2^{[1]} = \{12, 23\}$, $\mathcal{W}_1 = [\mathbb{I} - 0.1748(Z_1+Z_3) - 0.415Z_2 - 0.3426(X_1X_2+Y_1Y_2+X_2X_3+Y_2Y_3) + 0.0898(Z_1Z_2 + Z_2Z_3)]/8$, $\mathrm{Tr}(\mathcal{W}_1|\mathrm{W}_3\rangle\langle\mathrm{W}_3|) = -0.0285$, and $p_{\text{noise}} = 0.1859$;

2) $\mathcal{S}_2^{[2]} = \{12, 23, 13\}$, $\mathcal{W}_2 = [\mathbb{I} - 0.2516(Z_1+Z_2+Z_3) - 0.2377(X_1X_2+Y_1Y_2+X_2X_3+Y_2Y_3+X_1X_3+Y_1Y_3) + 0.2342(Z_1Z_2+Z_2Z_3+Z_1Z_3)]/8$, $\mathrm{Tr}(\mathcal{W}_2|\mathrm{W}_3\rangle\langle\mathrm{W}_3|) = -0.0546$, and $p_{\text{noise}} = 0.3039$.

EDL witnesses for the 4-qubit W state:

1) $\mathcal{S}_2^{[1]} = \{12, 23, 34\}$, $\mathcal{W}_1 = [\mathbb{I} - 0.2515(Z_2+Z_3) - 0.1341(Z_1+Z_4) - 0.2176(X_1X_2+Y_1Y_2+X_3X_4+Y_3Y_4) - 0.2542(X_2X_3+Y_2Y_3) - 0.0052(Z_1Z_2+Z_3Z_4) - 0.0885Z_2Z_3]/16$, $\mathrm{Tr}(\mathcal{W}_1|\mathrm{W}_4\rangle\langle\mathrm{W}_4|) = -0.0047$, and $p_{\text{noise}} = 0.0696$;

2) $\mathcal{S}_2^{[2]} = \{12, 23, 34, 24\}$, $\mathcal{W}_2 = [\mathbb{I} - 0.4166Z_2 - 0.1428Z_1 - 0.1782(Z_3+Z_4) - 0.2788(X_1X_2+Y_1Y_2) - 0.0104Z_1Z_2 - 0.1561(X_2X_3+Y_2Y_3+X_2X_4+Y_2Y_4) + 0.0429(Z_2Z_3+Z_2Z_4) - 0.0623(X_3X_4+Y_3Y_4) + 0.061Z_3Z_4]/16$, $\mathrm{Tr}(\mathcal{W}_2|\mathrm{W}_4\rangle\langle\mathrm{W}_4|) = -0.0070$, and $p_{\text{noise}} = 0.1001$;

3) $\mathcal{S}_2^{[3]} = \{12, 23, 34, 14\}$, $\mathcal{W}_3 = [\mathbb{I} - 0.2626(Z_1+Z_2+Z_3+Z_4) - 0.1548(X_1X_2+Y_1Y_2+X_2X_3+Y_2Y_3+X_3X_4+Y_3Y_4+X_1X_4+Y_1Y_4) + 0.078(Z_1Z_2+Z_2Z_3+Z_3Z_4+Z_1Z_4)]/16$, $\mathrm{Tr}(\mathcal{W}_3|\mathrm{W}_4\rangle\langle\mathrm{W}_4|) = -0.0090$, $p_{\text{noise}} = 0.1261$,

4) $\mathcal{S}_2^{[4]} = \{12, 23, 34, 24, 14\}$, $\mathcal{W}_4 = [\mathbb{I} - 0.303(Z_2+Z_4) - 0.219(Z_1+Z_3) - 0.1634(X_1X_2+Y_1Y_2+X_2X_3+Y_2Y_3+X_3X_4+Y_3Y_4+X_1X_4+Y_1Y_4) + 0.0503(Z_1Z_2+Z_2Z_3+Z_3Z_4+Z_1Z_4) + 0.0238(X_2X_4+Y_2Y_4) + 0.1544Z_2Z_4]/16$, $\mathrm{Tr}(\mathcal{W}_4|\mathrm{W}_4\rangle\langle\mathrm{W}_4|) = -0.0095$, and $p_{\text{noise}} = 0.1319$;

TABLE I. Comparative analysis of multiphoton entanglement state fidelities.

	History works		Our work
$\vert D_4\rangle$	Kiesel et al. (2007) [37]	0.844 ± 0.008	0.974 ± 0.004
	Chiuri et al. (2012) [44]	0.870 ± 0.010	
	Zhao et al. (2015) [45]	0.904 ± 0.004	
	Chen et al. (2023) [46]	0.817 ± 0.003	
$\vert W_3\rangle$	Lanyon et al. (2009) [47]	0.900 ± 0.030	0.982 ± 0.009
	Fang et al. (2019) [48]	0.920 ± 0.060	
	Li et al. (2020) [49]	0.866 ± 0.007	
	Kumar et al. (2023) [50]	0.873 ± 0.011	
$\vert C_4\rangle$	Kiesel et al. (2005) [51]	0.741 ± 0.013	0.968 ± 0.002
	Tokunaga et al. (2008) [52]	0.860 ± 0.015	
	Zhang et al. (2016) [53]	0.952 ± 0.003	
	Wu et al. (2021) [43]	0.945 ± 0.002	

TABLE II. Summary of EDL wintesses for the 3,4-qubit W states, the 4-qubit Dicke state, and the 4-qubit cluster state

States	Marginals	Witnesses	Expectation values	$p_{\text{noise}} =$
$\vert W_3\rangle$	$\mathcal{S}_2^{[1]} = \{12, 23\}$	$\mathcal{W}_1$	-0.0285	0.1859
	$\mathcal{S}_2^{[2]} = \{12, 23, 13\}$	$\mathcal{W}_2$	-0.0546	0.3039
$\vert W_4\rangle$	$\mathcal{S}_2^{[1]} = \{12, 23, 34\}$	$\mathcal{W}_1$	-0.0047	0.0696
	$\mathcal{S}_2^{[2]} = \{12, 23, 34, 24\}$	$\mathcal{W}_2$	-0.0070	0.1001
	$\mathcal{S}_2^{[3]} = \{12, 23, 34, 14\}$	$\mathcal{W}_3$	-0.0090	0.1261
	$\mathcal{S}_2^{[4]} = \{12, 23, 34, 24, 14\}$	$\mathcal{W}_4$	-0.0095	0.1319
	$\mathcal{S}_2^{[5]} = \{12, 23, 34, 14, 13, 24\}$	$\mathcal{W}_5$	-0.0114	0.1541
$\vert D_4\rangle$	$\mathcal{S}_2^{[1]} = \{12, 23, 34\}$	$\mathcal{W}_1$	-0.0065	0.0946
	$\mathcal{S}_2^{[2]} = \{12, 13, 14\}$	$\mathcal{W}_2$	-0.0093	0.1293
	$\mathcal{S}_2^{[3]} = \{12, 23, 34, 14\}$	$\mathcal{W}_3$	-0.0117	0.1577
	$\mathcal{S}_2^{[4]} = \{12, 23, 34, 24, 14\}$	$\mathcal{W}_4$	-0.0199	0.2413
	$\mathcal{S}_2^{[5]} = \{12, 23, 34, 14, 13, 24\}$	$\mathcal{W}_5$	-0.0285	0.3131
$\vert C_4\rangle$	$\mathcal{S}_3^{[1]} = \{123, 134\}$	$\mathcal{W}_1$	-0.0156	1/5
	$\mathcal{S}_3^{[2]} = \{123, 134\}$	$\mathcal{W}_2$	-0.0312	1/3
	$\mathcal{S}_3^{[3]} = \{123, 134, 234\}$	$\mathcal{W}_3$	-0.0417	2/5
	$\mathcal{S}_3^{[4]} = \{123, 124, 134, 234\}$	$\mathcal{W}_4$	-0.0625	1/2

5) $\mathcal{S}_2^{[5]} = \{12, 23, 34, 14, 13, 24\}$, $\mathcal{W}_5 = [\mathbb{I} - 0.2801(Z_1 + Z_2 + Z_3 + Z_4) - 0.1037(X_1X_2 + Y_1Y_2 + X_2X_3 + Y_2Y_3 + X_3X_4 + Y_3Y_4 + X_1X_4 + Y_1Y_4 + X_1X_3 + Y_1Y_3 + X_2X_4 + Y_2Y_4) + 0.0919(Z_1Z_2 + Z_2Z_3 + Z_3Z_4 + Z_1Z_4 + Z_1Z_3 + Z_2Z_4)]/16$, $\mathrm{Tr}\,(\mathcal{W}_5|\mathrm{W}_4\rangle\langle\mathrm{W}_4|) = -0.0114$, and $p_{\text{noise}} = 0.1541$.

EDL witnesses for the 4-qubit Dicke state:

1) $\mathcal{S}_2^{[1]} = \{12, 23, 34\}$, $\mathcal{W}_1 = [\mathbb{I} - 0.13(X_1X_2 + Y_1Y_2 + X_3X_4 + Y_3Y_4) - 0.5659(X_2X_3 + Y_2Y_3) + 0.1838(Z_1Z_2 + Z_3Z_4) - 0.3579Z_2Z_3]/16$, $\mathrm{Tr}\,(\mathcal{W}_1|\mathrm{D}_4\rangle\langle\mathrm{D}_4|) = -0.0065$, and $p_{\text{noise}} = 0.0946$;

2) $\mathcal{S}_2^{[2]} = \{12, 13, 14\}$, $\mathcal{W}_2 = [\mathbb{I} - 0.2711(X_1X_2 + Y_1Y_2 + X_1X_3 + Y_1Y_3 + X_1X_4 + Y_1Y_4) + 0.0641(Z_1Z_2 + Z_1Z_3 + Z_1Z_4)]/16$, $\mathrm{Tr}\,(\mathcal{W}_2|\mathrm{D}_4\rangle\langle\mathrm{D}_4|) = -0.0093$, and $p_{\text{noise}} < 0.1293$;

3) $\mathcal{S}_2^{[3]} = \{12, 23, 34, 14\}$, $\mathcal{W}_3 = [\mathbb{I} - 0.216(X_1X_2 + Y_1Y_2 + X_2X_3 + Y_2Y_3 + X_3X_4 + Y_3Y_4 + X_1X_4 + Y_1Y_4) + 0.0266(Z_1Z_2 + Z_2Z_3 + Z_3Z_4 + Z_1Z_4]/16$, $\mathrm{Tr}\,(\mathcal{W}_3|\mathrm{D}_4\rangle\langle\mathrm{D}_4|) = -0.0117$, and $p_{\text{noise}} < 0.1577$;

4) $\mathcal{S}_2^{[4]} = \{12, 23, 34, 24, 14\}$, $\mathcal{W}_4 = [\mathbb{I} - 0.1287(X_1X_2 + Y_1Y_2 + X_2X_3 + Y_2Y_3 + X_3X_4 + Y_3Y_4 + X_1X_4 + Y_1Y_4) + 0.2403(Z_1Z_2 + Z_2Z_3 + Z_3Z_4 + Z_1Z_4) - 0.1551(X_2X_4 +$

$Y_2Y_4) + 0.3132Z_2Z_4]/16$, $\mathrm{Tr}\,(\mathcal{W}_4|\mathrm{D}_4\rangle\langle\mathrm{D}_4|) = -0.0199$, and $p_{\text{noise}} = 0.2413$;

5) $\mathcal{S}_2^{[5]} = \{12, 23, 34, 14, 13, 24\}$, $\mathcal{W}_5 = [\mathbb{I} - 0.1228(X_1X_2 + Y_1Y_2 + X_2X_3 + Y_2Y_3 + X_3X_4 + Y_3Y_4 + X_1X_4 + Y_1Y_4 + X_1X_3 + Y_1Y_3 + X_2X_4 + Y_2Y_4) + 0.2368(Z_1Z_2 + Z_2Z_3 + Z_3Z_4 + Z_1Z_4 + Z_1Z_3 + Z_2Z_4)]/16$, $\mathrm{Tr}\,(\mathcal{W}_5|\mathrm{D}_4\rangle\langle\mathrm{D}_4|) = -0.0285$, and $p_{\text{noise}} = 0.3131$.

EDL witnesses for the 4-qubit Cluster state:

1) $\mathcal{S}_3^{[1]} = \{124, 134\}$, $\mathcal{W}_1 = [\mathbb{I} - 0.25(X_1X_2Z_4 - Y_1Y_2Z_4 + Z_3Z_4 + Z_1X_3X_4 - Z_1Y_3Y_4)]/16$, $\mathrm{Tr}(\mathcal{W}_1|\mathrm{C}_4\rangle\langle\mathrm{C}_4|) = -0.0156$, and $p_{\text{noise}} = 1/5$;

2) $\mathcal{S}_3^{[2]} = \{124, 134\}$, $\mathcal{W}_2 = [\mathbb{I} - 0.25(X_1X_2Z_4 - Y_1Y_2Z_4 + Z_1Z_2 + Z_3Z_4 + Z_1X_3X_4 - Z_1Y_3Y_4)]/16$, $\mathrm{Tr}(\mathcal{W}_2|\mathrm{C}_4\rangle\langle\mathrm{C}_4|) = -0.0312$, and $p_{\text{noise}} = 1/3$;

3) $\mathcal{S}_3^{[3]} = \{124, 134, 234\}$, $\mathcal{W}_3 = [\mathbb{I} + 0.1153Z_1Z_2 - 0.218Z_3Z_4 + 0.2243(Z_1Y_3Y_4 - Z_1X_3X_4 + Z_2Y_3Y_4 - Z_2X_3X_4) + 0.3333(Y_1Y_2Z_4 - X_1X_2Z_4)]/16$, $\mathrm{Tr}(\mathcal{W}_3|\mathrm{C}_4\rangle\langle\mathrm{C}_4|) = -0.0417$, and $p_{\text{noise}} = 2/5$;

4) $\mathcal{S}_3^{[4]} = \{123, 124, 134, 234\}$, $\mathcal{W}_4 = [\mathbb{I} + 0.0942(Z_1Z_2 + Z_3Z_4) + 0.2736(Y_1Y_2Z_3 - X_1X_2Z_3 + Y_1Y_2Z_4 - X_1X_2Z_4 + Z_1Y_3Y_4 - Z_1X_3X_4 + Z_2Y_3Y_4 - Z_2X_3X_4)]/16$, $\mathrm{Tr}(\mathcal{W}_4|\mathrm{C}_4\rangle\langle\mathrm{C}_4|) = -0.0625$, and $p_{\text{noise}} = 1/2$.

Appendix A: Determination of the state fidelity and projector witness.

To describe how the state $|\psi\rangle$ is prepared experimentally, we usually use the fidelity

$$F_{|\psi\rangle}(\rho) := \mathrm{Tr}(|\psi\rangle\langle\psi|\rho). \tag{A1}$$

So it is important to decompose $|\psi\rangle\langle\psi|$ using a small number of measurement settings. The projector witness is give by

$$\mathcal{W}_{\text{proj}} := \lambda_{|\psi\rangle}\mathbb{I} - |\psi\rangle\langle\psi|, \tag{A2}$$

where $\lambda_{|\psi\rangle}$ is the maximal squared Schmidt coefficient over all bipartitions [55]. If $F_{|\psi\rangle}(\rho) > \lambda_{|\psi\rangle}$, then ρ must be genuinely entangled.

1) The 3-qubit W state can be decomposed using five measurement settings [56]: $Z^{\otimes 3}$, $(Z \pm X)^{\otimes 3}$, $(Z \pm Y)^{\otimes 3}$, i.e.,

$$\begin{aligned}|\mathrm{W}_3\rangle\langle\mathrm{W}_3| = \frac{1}{24}[&-\mathbb{I} - 3(ZII + IZI + IIZ) - 5(ZZI + ZIZ + IZZ) - 7Z^{\otimes 3} \\ &+ (I + Z + X)^{\otimes 3} + (I + Z - X)^{\otimes 3} + (I + Z + Y)^{\otimes 3} + (I + Z - Y)^{\otimes 3}].\end{aligned} \tag{A3}$$

The projector witness is $\mathcal{W}_{\text{proj}} = \frac{2}{3}\mathbb{I} - |\mathrm{W}_3\rangle\langle\mathrm{W}_3|$.

2) The 4-qubit W state can be decomposed using seven measurement settings [57]: $X^{\otimes 4}$, $Y^{\otimes 4}$, $Z^{\otimes 4}$, $(Z \pm X)^{\otimes 4}$, $(Z \pm Y)^{\otimes 4}$, i.e.,

$$\begin{aligned}|\mathrm{W}_4\rangle\langle\mathrm{W}_4| = \frac{1}{64}[&-2(ZIII + IZII + IIZI + IIIZ) - 4(ZZII + ZIZI + ZIIZ + IZZI + IZIIZ + IIZZ) \\ &- 6(ZZZI + ZZIZ + ZIZZ + IZZZ) - 8Z^{\otimes 4} - 2X^{\otimes 4} - 2Y^{\otimes 4} \\ &+ (I + Z + X)^{\otimes 4} + (I + Z - X)^{\otimes 4} + (I + Z + Y)^{\otimes 4} + (I + Z - Y)^{\otimes 4}];\end{aligned} \tag{A4}$$

The projector witness is $\mathcal{W}_{\text{proj}} = \frac{3}{4}\mathbb{I} - |\mathrm{W}_4\rangle\langle\mathrm{W}_4|$.

3) The 4-qubit Dicke state can be decomposed using nine measurement settings [36]: $X^{\otimes 4}$, $Y^{\otimes 4}$, $Z^{\otimes 4}$, $(X \pm Y)^{\otimes 4}$, $(X \pm Z)^{\otimes 4}$, $(Y \pm Z)^{\otimes 4}$, i.e.,

$$\begin{aligned}|\mathrm{D}_4\rangle\langle\mathrm{D}_4| = \frac{1}{96}[&4X^{\otimes 4} + 2(X + I)^{\otimes 4} + 2(X - I)^{\otimes 4} + 4Y^{\otimes 4} + 2(Y + I)^{\otimes 4} + 2(Y - I)^{\otimes 4} + 16Z^{\otimes 4} - (Z + I)^{\otimes 4} \\ &- (Z - I)^{\otimes 4} - 2(X + Z)^{\otimes 4} - 2(X - Z)^{\otimes 4} - 2(Y + Z)^{\otimes 4} - 2(Y - Z)^{\otimes 4} + (X + Y)^{\otimes 4} + (X - Y)^{\otimes 4}].\end{aligned} \tag{A5}$$

The projector witness is $\mathcal{W}_{\text{proj}} = \frac{2}{3}\mathbb{I} - |\mathrm{D}_4\rangle\langle\mathrm{D}_4|$

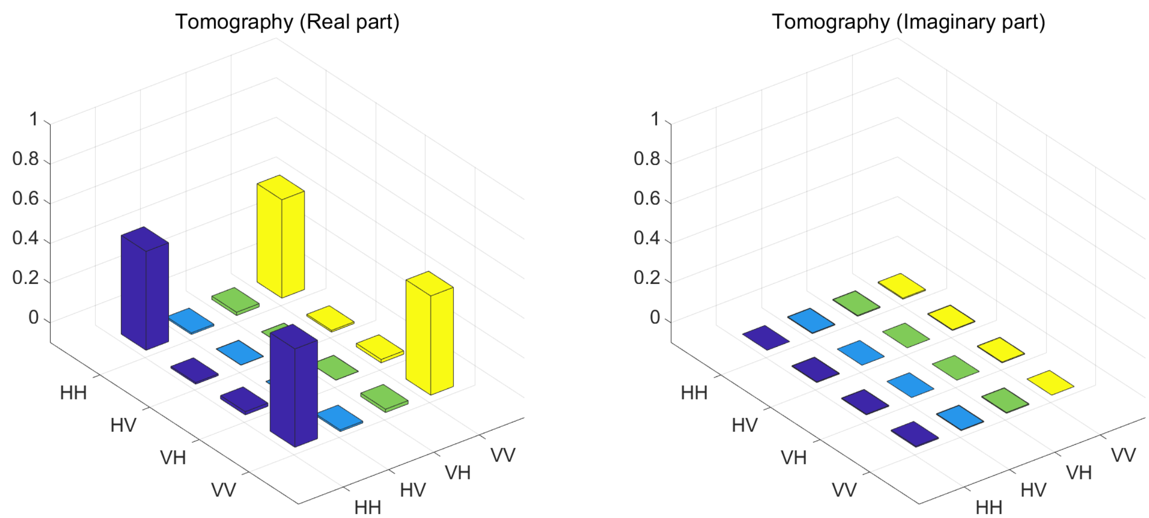

FIG. 5. Two-photon quantum state tomography of the entanglement source, which generate a state $|\psi>=\frac{1}{\sqrt{2}}(|HH\rangle+|VV\rangle)$. Realpart on the left, and imaginary part on the right.

4) The 4-qubit cluster state can be decomposed using nine measurement settings [58]: $Z^{\otimes 4}$, ZZXX, XXZZ, YYZZ, ZZYY, XYYX, YXXY, XYXY, YXYX i.e.,

$$|\mathrm{C}_4\rangle\langle\mathrm{C}_4| = \frac{1}{16}[\mathbb{I} + ZZII + XXZI + IZXX + IIZZ - YYZI + ZIXX + Z^{\otimes 4} + XYYX \\ + XXIZ - IZYY + YXYX - YYIZ - ZIYY + XYXY + YXXY]. \tag{A6}$$

The projector witness is $\mathcal{W}_{\text{proj}} = \frac{1}{2}\mathbb{I} - |\mathrm{C}_4\rangle\langle\mathrm{C}_4|$.

Appendix B: Experimental Details

1. Preparation of Entanglement Sources

To further validate the correctness of the EDL method, this work accomplished the preparation of multiple high-fidelity multiphoton entangled states, demonstrating significant improvements over previous studies. Table II presents a comparative analysis between representative works in multiphoton entanglement and our current achievements.

We developed a polarization-entangled photon source to generate high-fidelity four-photon W states and cluster states using the following configuration: A 775 nm pulsed pump laser (80 MHz repetition rate) with polarization state $|A\rangle$ was injected into an isosceles triangular Sagnac interferometer, where a dPBS (775/1550 nm) split the beam into counter-propagating components that pumped a ppKTP crystal to produce orthogonally polarized $|HV\rangle$ photon pairs at 1550 nm. When the clockwise and counter-clockwise paths were precisely overlapped, the parametric photons became path-indistinguishable at the PBS output ports, generating polarization-entangled state $|\psi>=\frac{1}{\sqrt{2}}(|HV\rangle+|VH\rangle)$, and converting to $|\psi>=\frac{1}{\sqrt{2}}(|HH\rangle+|VV\rangle)$ by a 45° HWP in one path mode. The two output modes were directly characterized via quantum state tomography using a measurement apparatus comprising QWPs, HWPs, and PBS. Under conditions of 1550±10 nm spectral filtering and 800 mW pump power, we measured an average two-photon coincidence rate of 60000 Hz in the $|H\rangle/|V\rangle$, $|A\rangle/|D\rangle$ and $|R\rangle/|L\rangle$ bases, achieving a two-photon fidelity [59] of 0.996±0.002. The quantum state tomography results for the two-photon entangled source are presented in Fig.5.

2. Four Photon Dicke State

To generate multiphoton entangled states with controlled fidelity, we systematically varied experimental conditions through the following approaches: (1) spectral filtering of parametric photons using different bandwidths (1550±5nm, 1550±10nm, or no filter); (2) precise temperature tuning of the ppKTP crystal via an electronic oven to modify spectral indistinguishability; (3) adjustment of walk-off compensation (KDP crystal angle) and optical path difference (via 1D translation stage) to control spatial indistinguishability.

The experimental configurations (measurement bases and conditions) for characterizing four-photon Dicke state the detailed configurations are shown in Tables III, and, and the results of fidelity and witness measurements are detailed in Tables IV, V, VI and VII.

TABLE III. Experimental configurations of four-photon Dicke state.

Fidelity	0.974 ± 0.004	0.951 ± 0.003	0.791 ± 0.002	0.510 ± 0.003
Spectral filtering	1550 ± 5 nm	1550 ± 10 nm	unfiltered	unfiltered
Pump Laser Power	300 mW	500 mW	2350 mW	2350 mW
PPKTP crystal temperature	25°C	25°C	92°C	92°C
Walk-off compensation	No offset	No offset	No offset	Offset of 9°
Rate of counting	0.20/s	1.60/s	270/s	270/s

TABLE IV. Experimental results of four-photon Dicke state fidelity and witness measurements under fidelity F = 0.974 ± 0.004. Including the required 27 operator expectation values.Under experimental configuration with parametric photon filtering at 1550±5 nm, 300 mW pump power, ppKTP crystal temperature stabilized at 25℃, and zero walk-off compensation offset. Each measurement basis accumulated approximately 3000 events over a 15000-second integration time. Error bars are derived from raw data analysis incorporating Poissonian counting statistics.

	Operators	Expectation value		Operators	Expectation value
1	X_1X_2	0.656 ± 0.014	15	Z_1Z_2	-0.368 ± 0.017
2	X_1X_3	0.659 ± 0.014	16	Z_1Z_3	-0.298 ± 0.017
3	X_1X_4	0.660 ± 0.014	17	Z_1Z_4	-0.328 ± 0.017
4	X_2X_3	0.662 ± 0.014	18	Z_2Z_3	-0.326 ± 0.017
5	X_2X_4	0.656 ± 0.014	19	Z_2Z_4	-0.296 ± 0.017
6	X_3X_4	0.650 ± 0.014	20	Z_3Z_4	-0.367 ± 0.017
7	$X_1X_2X_3X_4$	0.985 ± 0.003	21	$Z_1Z_2Z_3Z_4$	0.982 ± 0.003
8	Y_1Y_2	0.657 ± 0.014	22	$\left[\frac{1}{\sqrt{2}}(X+Z)\right]^{\otimes 4}$	-0.475 ± 0.016
9	Y_1Y_3	0.665 ± 0.014	23	$\left[\frac{1}{\sqrt{2}}(X-Z)\right]^{\otimes 4}$	-0.457 ± 0.016
10	Y_1Y_4	0.659 ± 0.014	24	$\left[\frac{1}{\sqrt{2}}(Y+Z)\right]^{\otimes 4}$	-0.419 ± 0.016
11	Y_2Y_3	0.660 ± 0.014	25	$\left[\frac{1}{\sqrt{2}}(Y-Z)\right]^{\otimes 4}$	-0.490 ± 0.016
12	Y_2Y_4	0.662 ± 0.014	26	$\left[\frac{1}{\sqrt{2}}(X+Y)\right]^{\otimes 4}$	0.979 ± 0.004
13	Y_3Y_4	0.647 ± 0.014	27	$\left[\frac{1}{\sqrt{2}}(X-Y)\right]^{\otimes 4}$	0.979 ± 0.004
14	$Y_1Y_2Y_3Y_4$	0.970 ± 0.005			
F_{D_4}		0.974 ± 0.004			
Witnesses		Experimental results		Theoretical expectation(F=1)	
$\mathcal{W}_1$		-0.00582 ± 0.00069		-0.0065	
$\mathcal{W}_2$		-0.00850 ± 0.00059		-0.0093	
$\mathcal{W}_3$		-0.0107 ± 0.0005		-0.0117	
$\mathcal{W}_4$		-0.0192 ± 0.0007		-0.0199	
$\mathcal{W}_5$		-0.0274 ± 0.0007		-0.0285	

TABLE V. Experimental results of four-photon Dicke state fidelity and witness measurements under fidelity F = 0.951 ± 0.003. Including the required 27 operator expectation values. Under experimental configuration with parametric photon filtering at 1550±10 nm, 500 mW pump power, ppKTP crystal temperature stabilized at 25°C, and zero walk-off compensation offset. Each measurement basis accumulated approximately 4000 events over a 2500-second integration time. Error bars are derived from raw data analysis incorporating Poissonian counting statistics.

	Operators	Expectation value		Operators	Expectation value
1	X_1X_2	0.684 ± 0.011	15	Z_1Z_2	-0.349 ± 0.015
2	X_1X_3	0.611 ± 0.012	16	Z_1Z_3	-0.347 ± 0.015
3	X_1X_4	0.626 ± 0.012	17	Z_1Z_4	-0.275 ± 0.015
4	X_2X_3	0.621 ± 0.012	18	Z_2Z_3	-0.278 ± 0.015
5	X_2X_4	0.606 ± 0.012	19	Z_2Z_4	-0.348 ± 0.015
6	X_3X_4	0.682 ± 0.011	20	Z_3Z_4	-0.347 ± 0.015
7	$X_1X_2X_3X_4$	0.952 ± 0.005	21	$Z_1Z_2Z_3Z_4$	0.945 ± 0.005
8	Y_1Y_2	0.676 ± 0.012	22	$\left[\frac{1}{\sqrt{2}}(X+Z)\right]^{\otimes 4}$	-0.430 ± 0.015
9	Y_1Y_3	0.636 ± 0.012	23	$\left[\frac{1}{\sqrt{2}}(X-Z)\right]^{\otimes 4}$	-0.453 ± 0.015
10	Y_1Y_4	0.615 ± 0.013	24	$\left[\frac{1}{\sqrt{2}}(Y+Z)\right]^{\otimes 4}$	-0.447 ± 0.014
11	Y_2Y_3	0.618 ± 0.013	25	$\left[\frac{1}{\sqrt{2}}(Y-Z)\right]^{\otimes 4}$	-0.461 ± 0.014
12	Y_2Y_4	0.635 ± 0.012	26	$\left[\frac{1}{\sqrt{2}}(X+Y)\right]^{\otimes 4}$	0.977 ± 0.003
13	Y_3Y_4	0.678 ± 0.012	27	$\left[\frac{1}{\sqrt{2}}(X-Y)\right]^{\otimes 4}$	0.960 ± 0.004
14	$Y_1Y_2Y_3Y_4$	0.966 ± 0.004			
F_{D_4}		0.951 ± 0.003			
Witnesses		Experimental results	Theoretical expectation(F=1)		
$\mathcal{W}_1$		-0.00517 ± 0.00076	-0.0065		
$\mathcal{W}_2$		-0.00659 ± 0.00051	-0.0093		
$\mathcal{W}_3$		-0.00977 ± 0.00046	-0.0117		
$\mathcal{W}_4$		-0.0169 ± 0.0006	-0.0199		
$\mathcal{W}_5$		-0.0253 ± 0.0006	-0.0285		

TABLE VI. Experimental results of four-photon Dicke state fidelity and witness under fidelity F = 0.791 ± 0.002. Including the required 27 operator expectation values. With no spectral filtering of parametric light, a pump laser power of 2350 mW, a ppKTP crystal temperature of 92℃, and no walk-off compensation offset, approximately 11,000 events were collected per measurement basis over a 40-second integration time. Error bars are derived from raw data analysis incorporating Poissonian counting statistics.

	Operators	Expectation value		Operators	Expectation value
1	X_1X_2	0.572 ± 0.008	15	Z_1Z_2	-0.351 ± 0.009
2	X_1X_3	0.542 ± 0.008	16	Z_1Z_3	-0.263 ± 0.009
3	X_1X_4	0.429 ± 0.009	17	Z_1Z_4	-0.372 ± 0.009
4	X_2X_3	0.555 ± 0.007	18	Z_2Z_3	-0.366 ± 0.008
5	X_2X_4	0.434 ± 0.009	19	Z_2Z_4	-0.262 ± 0.009
6	X_3X_4	0.396 ± 0.009	20	Z_3Z_4	-0.344 ± 0.009
7	$X_1X_2X_3X_4$	0.520 ± 0.008	21	$Z_1Z_2Z_3Z_4$	0.957 ± 0.003
8	Y_1Y_2	0.559 ± 0.008	22	$\left[\frac{1}{\sqrt{2}}(X+Z)\right]^{\otimes 4}$	-0.371 ± 0.009
9	Y_1Y_3	0.563 ± 0.008	23	$\left[\frac{1}{\sqrt{2}}(X-Z)\right]^{\otimes 4}$	-0.371 ± 0.009
10	Y_1Y_4	0.572 ± 0.007	24	$\left[\frac{1}{\sqrt{2}}(Y+Z)\right]^{\otimes 4}$	-0.377 ± 0.009
11	Y_2Y_3	0.567 ± 0.008	25	$\left[\frac{1}{\sqrt{2}}(Y-Z)\right]^{\otimes 4}$	-0.371 ± 0.009
12	Y_2Y_4	0.565 ± 0.008	26	$\left[\frac{1}{\sqrt{2}}(X+Y)\right]^{\otimes 4}$	0.704 ± 0.007
13	Y_3Y_4	0.560 ± 0.008	27	$\left[\frac{1}{\sqrt{2}}(X-Y)\right]^{\otimes 4}$	0.714 ± 0.007
14	$Y_1Y_2Y_3Y_4$	0.709 ± 0.007			
F_{D_4}		0.791 ± 0.002			
Witnesses		Experimental results		Theoretical expectation(F=1)	
$\mathcal{W}_1$		0.00610 ± 0.00048		-0.0065	
$\mathcal{W}_2$		0.00371 ± 0.00034		-0.0093	
$\mathcal{W}_3$		0.00330 ± 0.00031		-0.0117	
$\mathcal{W}_4$		-0.00767 ± 0.00039		-0.0199	
$\mathcal{W}_5$		-0.0149 ± 0.0004		-0.0285	

TABLE VII. Experimental results of four-photon Dicke state fidelity and witness under fidelity F = 0.510 ± 0.003. Including the required 27 operator expectation values. With no spectral filtering of parametric light, a pump laser power of 2350 mW, a ppKTP crystal temperature of 92°C, and walk-off compensation offset of 7°. Approximately 11,000 events were collected per measurement basis over a 40-second integration time. Error bars are derived from raw data analysis incorporating Poissonian counting statistics.

	Operators	Expectation value		Operators	Expectation value
1	X_1X_2	0.418 ± 0.009	15	Z_1Z_2	-0.267 ± 0.009
2	X_1X_3	0.403 ± 0.009	16	Z_1Z_3	-0.213 ± 0.009
3	X_1X_4	0.419 ± 0.009	17	Z_1Z_4	-0.275 ± 0.009
4	X_2X_3	0.412 ± 0.009	18	Z_2Z_3	-0.274 ± 0.009
5	X_2X_4	0.442 ± 0.009	19	Z_2Z_4	-0.206 ± 0.009
6	X_3X_4	0.417 ± 0.009	20	Z_3Z_4	-0.257 ± 0.009
7	$X_1X_2X_3X_4$	0.336 ± 0.009	21	$Z_1Z_2Z_3Z_4$	0.542 ± 0.008
8	Y_1Y_2	0.413 ± 0.009	22	$\left[\frac{1}{\sqrt{2}}(X+Z)\right]^{\otimes 4}$	-0.100 ± 0.010
9	Y_1Y_3	0.398 ± 0.009	23	$\left[\frac{1}{\sqrt{2}}(X-Z)\right]^{\otimes 4}$	-0.173 ± 0.010
10	Y_1Y_4	0.418 ± 0.009	24	$\left[\frac{1}{\sqrt{2}}(Y+Z)\right]^{\otimes 4}$	-0.062 ± 0.010
11	Y_2Y_3	0.408 ± 0.009	25	$\left[\frac{1}{\sqrt{2}}(Y-Z)\right]^{\otimes 4}$	-0.173 ± 0.010
12	Y_2Y_4	0.431 ± 0.009	26	$\left[\frac{1}{\sqrt{2}}(X+Y)\right]^{\otimes 4}$	0.256 ± 0.009
13	Y_3Y_4	0.405 ± 0.009	27	$\left[\frac{1}{\sqrt{2}}(X-Y)\right]^{\otimes 4}$	0.469 ± 0.009
14	$Y_1Y_2Y_3Y_4$	0.350 ± 0.009			
F_{D_4}		0.510 ± 0.003			
Witnesses		Experimental results		Theoretical expectation(F=1)	
$\mathcal{W}_1$		0.0202 ± 0.0005		-0.0065	
$\mathcal{W}_2$		0.0176 ± 0.0004		-0.0093	
$\mathcal{W}_3$		0.0160 ± 0.0003		-0.0117	
$\mathcal{W}_4$		0.00729 ± 0.00040		-0.0199	
$\mathcal{W}_5$		0.00219 ± 0.00041		-0.0285	

3. Three Photon W State

The detailed configurations are shown in Tables VIII, and results for measuring the fidelity and witness of the three-photon W state are presented in Tables IX, X and XI.

TABLE VIII. Experimental configurations of three-photon W state.

Fidelity	0.982 ± 0.009	0.777 ± 0.004	0.337 ± 0.009
Spectral filtering	1550 ± 10 nm	unfiltered	unfiltered
Pump Laser Power	600 mW	2350 mW	2350 mW
PPKTP crystal temperature	25°C	93°C	93°C
Walk-off compensation	No offset	No offset	offset of 15°
Rate of counting	1.10/s	140/s	135/s

TABLE IX. Experimental results of three-photon W state fidelity and witness under fidelity F = 0.982 ± 0.009. Including the required 41 operator expectation values. Under the conditions of a parametric light filtering wavelength of 1550±10nm, a pump laser power of 600mw, a PPKTP crystal temperature of 25℃, and walk-off compensation without offset, the data acquisition time for each basis vector is approximately 3600s, with 3800 events collected. Error bars are derived from raw data analysis incorporating Poissonian counting statistics.

	Operators	Expectation value		Operators	Expectation value
1	Z_1	-0.270 ± 0.015	22	$\left[\frac{1}{\sqrt{2}}(Z+Y)\right]_1$	-0.211 ± 0.016
2	Z_2	-0.365 ± 0.014	23	$\left[\frac{1}{\sqrt{2}}(Z+Y)\right]_2$	-0.293 ± 0.016
3	Z_3	-0.341 ± 0.015	24	$\left[\frac{1}{\sqrt{2}}(Z+Y)\right]_3$	-0.217 ± 0.016
4	Z_1Z_2	-0.333 ± 0.015	25	$\left[\frac{1}{\sqrt{2}}(Z+Y)\right]_1\left[\frac{1}{\sqrt{2}}(Z+Y)\right]_2$	0.159 ± 0.016
5	Z_1Z_3	-0.370 ± 0.014	26	$\left[\frac{1}{\sqrt{2}}(Z+Y)\right]_1\left[\frac{1}{\sqrt{2}}(Z+Y)\right]_3$	0.149 ± 0.016
6	Z_2Z_3	-0.270 ± 0.015	27	$\left[\frac{1}{\sqrt{2}}(Z+Y)\right]_2\left[\frac{1}{\sqrt{2}}(Z+Y)\right]_3$	0.146 ± 0.016
7	$Z_1Z_2Z_3$	0.950 ± 0.005	28	$\left[\frac{1}{\sqrt{2}}(Z-Y)\right]^{\otimes 3}$	-0.309 ± 0.016
8	$\left[\frac{1}{\sqrt{2}}(Z+X)\right]_1$	-0.208 ± 0.016	29	$\left[\frac{1}{\sqrt{2}}(Z-Y)\right]_1$	-0.236 ± 0.016
9	$\left[\frac{1}{\sqrt{2}}(Z+X)\right]_2$	-0.236 ± 0.015	30	$\left[\frac{1}{\sqrt{2}}(Z-Y)\right]_2$	-0.264 ± 0.016
10	$\left[\frac{1}{\sqrt{2}}(Z+X)\right]_3$	-0.218 ± 0.016	31	$\left[\frac{1}{\sqrt{2}}(Z-Y)\right]_3$	-0.241 ± 0.016
11	$\left[\frac{1}{\sqrt{2}}(Z+X)\right]_1\left[\frac{1}{\sqrt{2}}(Z+X)\right]_2$	0.203 ± 0.016	32	$\left[\frac{1}{\sqrt{2}}(Z-Y)\right]_1\left[\frac{1}{\sqrt{2}}(Z-Y)\right]_2$	0.192 ± 0.016
12	$\left[\frac{1}{\sqrt{2}}(Z+X)\right]_1\left[\frac{1}{\sqrt{2}}(Z+X)\right]_3$	0.193 ± 0.016	33	$\left[\frac{1}{\sqrt{2}}(Z-Y)\right]_1\left[\frac{1}{\sqrt{2}}(Z-Y)\right]_3$	0.169 ± 0.016
13	$\left[\frac{1}{\sqrt{2}}(Z+X)\right]_2\left[\frac{1}{\sqrt{2}}(Z+X)\right]_3$	0.196 ± 0.016	34	$\left[\frac{1}{\sqrt{2}}(Z-Y)\right]_2\left[\frac{1}{\sqrt{2}}(Z-Y)\right]_3$	0.168 ± 0.016
14	$\left[\frac{1}{\sqrt{2}}(Z+X)\right]^{\otimes 3}$	-0.422 ± 0.014	35	$\left[\frac{1}{\sqrt{2}}(Z-Y)\right]^{\otimes 3}$	-0.335 ± 0.015
15	$\left[\frac{1}{\sqrt{2}}(Z-X)\right]_1$	-0.249 ± 0.016	36	X_1X_2	0.677 ± 0.011
16	$\left[\frac{1}{\sqrt{2}}(Z-X)\right]_2$	-0.260 ± 0.016	37	X_1X_3	0.614 ± 0.012
17	$\left[\frac{1}{\sqrt{2}}(Z-X)\right]_3$	-0.254 ± 0.016	38	X_2X_3	0.602 ± 0.012
18	$\left[\frac{1}{\sqrt{2}}(Z-X)\right]_1\left[\frac{1}{\sqrt{2}}(Z-X)\right]_2$	0.170 ± 0.016	39	Y_1Y_2	0.676 ± 0.013
19	$\left[\frac{1}{\sqrt{2}}(Z-X)\right]_1\left[\frac{1}{\sqrt{2}}(Z-X)\right]_3$	0.154 ± 0.016	40	Y_1Y_3	0.687 ± 0.012
20	$\left[\frac{1}{\sqrt{2}}(Z-X)\right]_2\left[\frac{1}{\sqrt{2}}(Z-X)\right]_3$	0.127 ± 0.016	41	Y_2Y_3	0.676 ± 0.013
21	$\left[\frac{1}{\sqrt{2}}(Z-X)\right]^{\otimes 3}$	-0.293 ± 0.016	42	I	1
F_{W_3}		0.982 ± 0.009			
Witnesses		Experimental results		Theoretical expectation(F=1)	
$\mathcal{W}_1$		-0.027 ± 0.001		-0.029	
$\mathcal{W}_2$		-0.051 ± 0.001		-0.055	

TABLE X. Experimental results of three-photon W state fidelity and witness under fidelity F = 0.777 ± 0.004. Including the required 41 operator expectation values. Under the conditions of unfiltered parametric light, a pump laser power of 2350mw, a PPKTP crystal temperature of 93℃, and no walk-off compensation offset, data were collected for each basis vector over approximately 180s with 25,000 events. Error bars are derived from raw data analysis incorporating Poissonian counting statistics.

	Operators	Expectation value		Operators	Expectation value
1	Z_1	-0.315 ± 0.006	22	$\left[\frac{1}{\sqrt{2}}(Z+Y)\right]_1$	-0.233 ± 0.006
2	Z_2	-0.349 ± 0.006	23	$\left[\frac{1}{\sqrt{2}}(Z+Y)\right]_2$	-0.248 ± 0.006
3	Z_3	-0.314 ± 0.006	24	$\left[\frac{1}{\sqrt{2}}(Z+Y)\right]_3$	-0.241 ± 0.006
4	Z_1Z_2	-0.318 ± 0.006	25	$\left[\frac{1}{\sqrt{2}}(Z+Y)\right]_1\left[\frac{1}{\sqrt{2}}(Z+Y)\right]_2$	0.078 ± 0.006
5	Z_1Z_3	-0.350 ± 0.006	26	$\left[\frac{1}{\sqrt{2}}(Z+Y)\right]_1\left[\frac{1}{\sqrt{2}}(Z+Y)\right]_3$	0.081 ± 0.006
6	Z_2Z_3	-0.311 ± 0.006	27	$\left[\frac{1}{\sqrt{2}}(Z+Y)\right]_2\left[\frac{1}{\sqrt{2}}(Z+Y)\right]_3$	0.074 ± 0.006
7	$Z_1Z_2Z_3$	0.956 ± 0.002	28	$\left[\frac{1}{\sqrt{2}}(Z-Y)\right]^{\otimes 3}$	-0.139 ± 0.006
8	$\left[\frac{1}{\sqrt{2}}(Z+X)\right]_1$	-0.233 ± 0.006	29	$\left[\frac{1}{\sqrt{2}}(Z-Y)\right]_1$	-0.254 ± 0.006
9	$\left[\frac{1}{\sqrt{2}}(Z+X)\right]_2$	-0.251 ± 0.006	30	$\left[\frac{1}{\sqrt{2}}(Z-Y)\right]_2$	-0.243 ± 0.006
10	$\left[\frac{1}{\sqrt{2}}(Z+X)\right]_3$	-0.236 ± 0.006	31	$\left[\frac{1}{\sqrt{2}}(Z-Y)\right]_3$	-0.229 ± 0.006
11	$\left[\frac{1}{\sqrt{2}}(Z+X)\right]_1\left[\frac{1}{\sqrt{2}}(Z+X)\right]_2$	0.093 ± 0.006	32	$\left[\frac{1}{\sqrt{2}}(Z-Y)\right]_1\left[\frac{1}{\sqrt{2}}(Z-Y)\right]_2$	0.052 ± 0.006
12	$\left[\frac{1}{\sqrt{2}}(Z+X)\right]_1\left[\frac{1}{\sqrt{2}}(Z+X)\right]_3$	0.089 ± 0.006	33	$\left[\frac{1}{\sqrt{2}}(Z-Y)\right]_1\left[\frac{1}{\sqrt{2}}(Z-Y)\right]_3$	0.048 ± 0.006
13	$\left[\frac{1}{\sqrt{2}}(Z+X)\right]_2\left[\frac{1}{\sqrt{2}}(Z+X)\right]_3$	0.087 ± 0.006	34	$\left[\frac{1}{\sqrt{2}}(Z-Y)\right]_2\left[\frac{1}{\sqrt{2}}(Z-Y)\right]_3$	0.060 ± 0.006
14	$\left[\frac{1}{\sqrt{2}}(Z+X)\right]^{\otimes 3}$	-0.156 ± 0.006	35	$\left[\frac{1}{\sqrt{2}}(Z-Y)\right]^{\otimes 3}$	-0.092 ± 0.006
15	$\left[\frac{1}{\sqrt{2}}(Z-X)\right]_1$	-0.236 ± 0.006	36	X_1X_2	0.437 ± 0.006
16	$\left[\frac{1}{\sqrt{2}}(Z-X)\right]_2$	-0.259 ± 0.006	37	X_1X_3	0.440 ± 0.006
17	$\left[\frac{1}{\sqrt{2}}(Z-X)\right]_3$	-0.238 ± 0.006	38	X_2X_3	0.438 ± 0.006
18	$\left[\frac{1}{\sqrt{2}}(Z-X)\right]_1\left[\frac{1}{\sqrt{2}}(Z-X)\right]_2$	0.059 ± 0.006	39	Y_1Y_2	0.449 ± 0.006
19	$\left[\frac{1}{\sqrt{2}}(Z-X)\right]_1\left[\frac{1}{\sqrt{2}}(Z-X)\right]_3$	0.035 ± 0.006	40	Y_1Y_3	0.452 ± 0.006
20	$\left[\frac{1}{\sqrt{2}}(Z-X)\right]_2\left[\frac{1}{\sqrt{2}}(Z-X)\right]_3$	0.035 ± 0.006	41	Y_2Y_3	0.438 ± 0.006
21	$\left[\frac{1}{\sqrt{2}}(Z-X)\right]^{\otimes 3}$	-0.081 ± 0.006	42	I	1
F_{W_3}		0.777 ± 0.004			
Witnesses		Experimental results		Theoretical expectation(F=1)	
$\mathcal{W}_1$		0.011 ± 0.001		-0.029	
$\mathcal{W}_2$		-0.013 ± 0.001		-0.055	

TABLE XI. Experimental results of three-photon W state fidelity and witness under fidelity F = 0.337 ± 0.009. Including the required 41 operator expectation values. Under the conditions of unfiltered parametric light, a pump laser power of 2350mw, a PPKTP crystal temperature of 93℃, and no walk-off compensation offset of 15°, data were collected for each basis vector over approximately 180s with 25,000 events. Error bars are derived from raw data analysis incorporating Poissonian counting statistics.

	Operators	Expectation value		Operators	Expectation value
1	Z_1	-0.033 ± 0.014	22	$\left[\frac{1}{\sqrt{2}}(Z+Y)\right]_1$	-0.228 ± 0.013
2	Z_2	-0.077 ± 0.014	23	$\left[\frac{1}{\sqrt{2}}(Z+Y)\right]_2$	-0.239 ± 0.013
3	Z_3	-0.040 ± 0.014	24	$\left[\frac{1}{\sqrt{2}}(Z+Y)\right]_3$	-0.218 ± 0.013
4	Z_1Z_2	-0.041 ± 0.014	25	$\left[\frac{1}{\sqrt{2}}(Z+Y)\right]_1\left[\frac{1}{\sqrt{2}}(Z+Y)\right]_2$	-0.076 ± 0.014
5	Z_1Z_3	-0.053 ± 0.014	26	$\left[\frac{1}{\sqrt{2}}(Z+Y)\right]_1\left[\frac{1}{\sqrt{2}}(Z+Y)\right]_3$	-0.069 ± 0.014
6	Z_2Z_3	-0.039 ± 0.014	27	$\left[\frac{1}{\sqrt{2}}(Z+Y)\right]_2\left[\frac{1}{\sqrt{2}}(Z+Y)\right]_3$	-0.067 ± 0.014
7	$Z_1Z_2Z_3$	-0.152 ± 0.014	28	$\left[\frac{1}{\sqrt{2}}(Z-Y)\right]^{\otimes 3}$	0.152 ± 0.014
8	$\left[\frac{1}{\sqrt{2}}(Z+X)\right]_1$	-0.219 ± 0.013	29	$\left[\frac{1}{\sqrt{2}}(Z-Y)\right]_1$	0.156 ± 0.014
9	$\left[\frac{1}{\sqrt{2}}(Z+X)\right]_2$	-0.222 ± 0.013	30	$\left[\frac{1}{\sqrt{2}}(Z-Y)\right]_2$	0.135 ± 0.014
10	$\left[\frac{1}{\sqrt{2}}(Z+X)\right]_3$	-0.201 ± 0.013	31	$\left[\frac{1}{\sqrt{2}}(Z-Y)\right]_3$	0.152 ± 0.014
11	$\left[\frac{1}{\sqrt{2}}(Z+X)\right]_1\left[\frac{1}{\sqrt{2}}(Z+X)\right]_2$	-0.033 ± 0.014	32	$\left[\frac{1}{\sqrt{2}}(Z-Y)\right]_1\left[\frac{1}{\sqrt{2}}(Z-Y)\right]_2$	0.475 ± 0.012
12	$\left[\frac{1}{\sqrt{2}}(Z+X)\right]_1\left[\frac{1}{\sqrt{2}}(Z+X)\right]_3$	-0.022 ± 0.014	33	$\left[\frac{1}{\sqrt{2}}(Z-Y)\right]_1\left[\frac{1}{\sqrt{2}}(Z-Y)\right]_3$	0.483 ± 0.012
13	$\left[\frac{1}{\sqrt{2}}(Z+X)\right]_2\left[\frac{1}{\sqrt{2}}(Z+X)\right]_3$	-0.016 ± 0.014	34	$\left[\frac{1}{\sqrt{2}}(Z-Y)\right]_2\left[\frac{1}{\sqrt{2}}(Z-Y)\right]_3$	0.486 ± 0.012
14	$\left[\frac{1}{\sqrt{2}}(Z+X)\right]^{\otimes 3}$	0.069 ± 0.014	35	$\left[\frac{1}{\sqrt{2}}(Z-Y)\right]^{\otimes 3}$	-0.111 ± 0.014
15	$\left[\frac{1}{\sqrt{2}}(Z-X)\right]_1$	0.118 ± 0.014	36	X_1X_2	0.483 ± 0.012
16	$\left[\frac{1}{\sqrt{2}}(Z-X)\right]_2$	0.120 ± 0.014	37	X_1X_3	0.483 ± 0.012
17	$\left[\frac{1}{\sqrt{2}}(Z-X)\right]_3$	0.144 ± 0.013	38	X_2X_3	0.470 ± 0.012
18	$\left[\frac{1}{\sqrt{2}}(Z-X)\right]_1\left[\frac{1}{\sqrt{2}}(Z-X)\right]_2$	0.471 ± 0.012	39	Y_1Y_2	0.422 ± 0.013
19	$\left[\frac{1}{\sqrt{2}}(Z-X)\right]_1\left[\frac{1}{\sqrt{2}}(Z-X)\right]_3$	0.470 ± 0.012	40	Y_1Y_3	0.440 ± 0.012
20	$\left[\frac{1}{\sqrt{2}}(Z-X)\right]_2\left[\frac{1}{\sqrt{2}}(Z-X)\right]_3$	0.472 ± 0.012	41	Y_2Y_3	0.447 ± 0.012
21	$\left[\frac{1}{\sqrt{2}}(Z-X)\right]^{\otimes 3}$	-0.143 ± 0.013	42	I	1
F_{W_3}		0.337 ± 0.009			
Witnesses		Experimental results		Theoretical expectation(F=1)	
$\mathcal{W}_1$		0.040 ± 0.001		-0.029	
$\mathcal{W}_2$		0.035 ± 0.001		-0.055	

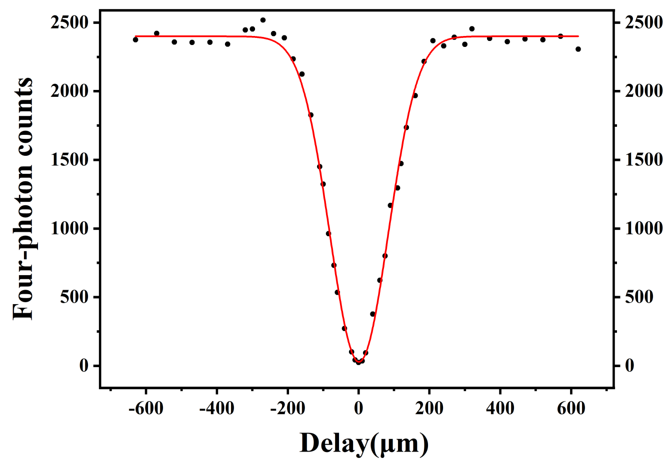

FIG. 6. HOM interference curve. By adjusting the one-dimensional displacement stage, the delay amount at the offset center of the displacement stage is plotted as the horizontal coordinate, and the four-body coincidence count within 1200s is plotted as the vertical coordinate; the entanglement source laser pump power is 300mw, and the directly pumped SPDC source power is 319mw. During measurement, 1550±10nm filtering is performed.

4. Four Photon W State

In the preparation of the four-photon W state, the photon pairs $|HH\rangle$ in spatial mode 3 and the photons $\frac{1}{\sqrt{2}}(|H\rangle + |V\rangle)$ in spatial mode 2 need to simultaneously arrive at the beam splitter (BS) in a superposition mode. The half-wave plate (HWP) before the entanglement source dPBS and the HWP before the interference BS are adjusted so that both sources contribute an H photon at the BS. We performed Hong-Ou-Mandel quantum interference [60] between the entanglement source and the directly pumped spontaneous parametric down-conversion (SPDC) source to test the indistinguishability of the two photons in spatial and frequency modes at the BS, thereby ensuring the consistency of the optical paths of the two spatial modes during state preparation. As shown in Figure 6, at zero delay, a dip appears in the quadruple coincidence count, and the measured interference visibility is 0.989 ± 0.004. The detailed configurations are shown in Tables XII, and the measurement results of the fidelity and witness of the four-photon W state are shown in Tables XIII, XIV, and XV.

TABLE XII. Experimental configurations of four-photon W state.

Fidelity	0.971 ± 0.006	0.919 ± 0.004	0.720 ± 0.004
Spectral filtering	1550 ± 10 nm	unfiltered	unfiltered
Pump Laser Power of entangled source	200 mW	1000 mW	1000 mW
Pump Laser Power of direct SPDC	400 mW	1200 mW	1200 mW
PPKTP crystal temperature (both)	25°C	70°C	70°C
Walk-off compensation	No offset	No offset	offset of 15°
interference optical range difference	0	0	40 μm
Rate of counting	0.20/s	21/s	25/s

TABLE XIII. Experimental results of four-photon W state fidelity and witness under fidelity F = 0.971 ± 0.006. Including the required 90 operator expectation values. Under the conditions of 1550±10nm filtered parametric light, pump power of entangled source in 200mw, and direct SPDC source in 400mw, PPKTP crystal temperature of 25℃, and no walk-off compensation offset, no path difference in BS interference. X/Y/Z bases: 30,000 s (6,600 events). Other bases: 10,000 s (2,300 events). Error bars are derived from raw data analysis incorporating Poissonian counting statistics.

	Operators	Expectation value		Operators	Expectation value		Operators	Expectation value
1	Z_1	0.546 ± 0.010	31	$\left[\frac{1}{\sqrt{2}}(Z+X)\right]_{2,3,4}$	0.345 ± 0.019	61	$\left[\frac{1}{\sqrt{2}}(Z+Y)\right]_{2,3,4}$	0.310 ± 0.020
2	Z_2	0.473 ± 0.011	32	$\left[\frac{1}{\sqrt{2}}(Z+X)\right]^{\otimes 4}$	0.455 ± 0.018	62	$\left[\frac{1}{\sqrt{2}}(Z+Y)\right]^{\otimes 4}$	0.500 ± 0.018
3	Z_3	0.520 ± 0.011	33	$\left[\frac{1}{\sqrt{2}}(Z-X)\right]_{1}$	0.377 ± 0.018	63	$\left[\frac{1}{\sqrt{2}}(Z-Y)\right]_{1}$	0.365 ± 0.019
4	Z_4	0.449 ± 0.011	34	$\left[\frac{1}{\sqrt{2}}(Z-X)\right]_{2}$	0.353 ± 0.019	64	$\left[\frac{1}{\sqrt{2}}(Z-Y)\right]_{2}$	0.371 ± 0.019
5	Z_1Z_2	0.031 ± 0.012	35	$\left[\frac{1}{\sqrt{2}}(Z-X)\right]_{3}$	0.353 ± 0.019	65	$\left[\frac{1}{\sqrt{2}}(Z-Y)\right]_{3}$	0.386 ± 0.019
6	Z_1Z_3	0.076 ± 0.012	36	$\left[\frac{1}{\sqrt{2}}(Z-X)\right]_{4}$	0.386 ± 0.018	66	$\left[\frac{1}{\sqrt{2}}(Z-Y)\right]_{4}$	0.320 ± 0.019
7	Z_1Z_4	0.000 ± 0.012	37	$\left[\frac{1}{\sqrt{2}}(Z-X)\right]_{1,2}$	0.266 ± 0.019	67	$\left[\frac{1}{\sqrt{2}}(Z-Y)\right]_{1,2}$	0.262 ± 0.019
8	Z_2Z_3	0.004 ± 0.012	38	$\left[\frac{1}{\sqrt{2}}(Z-X)\right]_{1,3}$	0.277 ± 0.019	68	$\left[\frac{1}{\sqrt{2}}(Z-Y)\right]_{1,3}$	0.264 ± 0.019
9	Z_2Z_4	-0.069 ± 0.012	39	$\left[\frac{1}{\sqrt{2}}(Z-X)\right]_{1,4}$	0.206 ± 0.020	69	$\left[\frac{1}{\sqrt{2}}(Z-Y)\right]_{1,4}$	0.216 ± 0.020
10	Z_3Z_4	-0.027 ± 0.012	40	$\left[\frac{1}{\sqrt{2}}(Z-X)\right]_{2,3}$	0.249 ± 0.020	70	$\left[\frac{1}{\sqrt{2}}(Z-Y)\right]_{2,3}$	0.251 ± 0.020
11	$Z_1Z_2Z_3$	-0.444 ± 0.011	41	$\left[\frac{1}{\sqrt{2}}(Z-X)\right]_{2,4}$	0.180 ± 0.020	71	$\left[\frac{1}{\sqrt{2}}(Z-Y)\right]_{2,4}$	0.226 ± 0.020
12	$Z_1Z_2Z_4$	-0.509 ± 0.011	42	$\left[\frac{1}{\sqrt{2}}(Z-X)\right]_{3,4}$	0.238 ± 0.019	72	$\left[\frac{1}{\sqrt{2}}(Z-Y)\right]_{3,4}$	0.211 ± 0.020
13	$Z_1Z_3Z_4$	-0.467 ± 0.011	43	$\left[\frac{1}{\sqrt{2}}(Z-X)\right]_{1,2,3}$	0.348 ± 0.019	73	$\left[\frac{1}{\sqrt{2}}(Z-Y)\right]_{1,2,3}$	0.326 ± 0.019
14	$Z_2Z_3Z_4$	-0.535 ± 0.011	44	$\left[\frac{1}{\sqrt{2}}(Z-X)\right]_{1,2,4}$	0.311 ± 0.019	74	$\left[\frac{1}{\sqrt{2}}(Z-Y)\right]_{1,2,4}$	0.328 ± 0.019
15	$Z^{\otimes 4}$	-0.981 ± 0.002	45	$\left[\frac{1}{\sqrt{2}}(Z-X)\right]_{1,3,4}$	0.305 ± 0.019	75	$\left[\frac{1}{\sqrt{2}}(Z-Y)\right]_{1,3,4}$	0.340 ± 0.019
16	$X^{\otimes 4}$	0.007 ± 0.012	46	$\left[\frac{1}{\sqrt{2}}(Z-X)\right]_{2,3,4}$	0.303 ± 0.019	76	$\left[\frac{1}{\sqrt{2}}(Z-Y)\right]_{2,3,4}$	0.288 ± 0.019
17	$Y^{\otimes 4}$	0.004 ± 0.012	47	$\left[\frac{1}{\sqrt{2}}(Z-X)\right]^{\otimes 4}$	0.472 ± 0.018	77	$\left[\frac{1}{\sqrt{2}}(Z-Y)\right]^{\otimes 4}$	0.474 ± 0.018
18	$\left[\frac{1}{\sqrt{2}}(Z+X)\right]_{1}$	0.366 ± 0.019	48	$\left[\frac{1}{\sqrt{2}}(Z+Y)\right]_{1}$	0.324 ± 0.020	78	X_1X_2	0.469 ± 0.011
19	$\left[\frac{1}{\sqrt{2}}(Z+X)\right]_{2}$	0.330 ± 0.019	49	$\left[\frac{1}{\sqrt{2}}(Z+Y)\right]_{2}$	0.346 ± 0.020	79	Y_1Y_2	0.474 ± 0.011
20	$\left[\frac{1}{\sqrt{2}}(Z+X)\right]_{3}$	0.349 ± 0.019	50	$\left[\frac{1}{\sqrt{2}}(Z+Y)\right]_{3}$	0.341 ± 0.020	80	X_2X_3	0.486 ± 0.011
21	$\left[\frac{1}{\sqrt{2}}(Z+X)\right]_{4}$	0.309 ± 0.020	51	$\left[\frac{1}{\sqrt{2}}(Z+Y)\right]_{4}$	0.353 ± 0.020	81	Y_2Y_3	0.491 ± 0.011
22	$\left[\frac{1}{\sqrt{2}}(Z+X)\right]_{1,2}$	0.252 ± 0.020	52	$\left[\frac{1}{\sqrt{2}}(Z+Y)\right]_{1,2}$	0.263 ± 0.020	82	X_3X_4	0.506 ± 0.010
23	$\left[\frac{1}{\sqrt{2}}(Z+X)\right]_{1,3}$	0.262 ± 0.020	53	$\left[\frac{1}{\sqrt{2}}(Z+Y)\right]_{1,3}$	0.277 ± 0.020	83	Y_3Y_4	0.500 ± 0.011
24	$\left[\frac{1}{\sqrt{2}}(Z+X)\right]_{1,4}$	0.221 ± 0.020	54	$\left[\frac{1}{\sqrt{2}}(Z+Y)\right]_{1,4}$	0.242 ± 0.020	84	X_1X_4	0.473 ± 0.011
25	$\left[\frac{1}{\sqrt{2}}(Z+X)\right]_{2,3}$	0.249 ± 0.020	55	$\left[\frac{1}{\sqrt{2}}(Z+Y)\right]_{2,3}$	0.242 ± 0.020	85	Y_1Y_4	0.470 ± 0.011
26	$\left[\frac{1}{\sqrt{2}}(Z+X)\right]_{2,4}$	0.303 ± 0.020	56	$\left[\frac{1}{\sqrt{2}}(Z+Y)\right]_{2,4}$	0.208 ± 0.020	86	X_1X_3	0.483 ± 0.011
27	$\left[\frac{1}{\sqrt{2}}(Z+X)\right]_{3,4}$	0.253 ± 0.020	57	$\left[\frac{1}{\sqrt{2}}(Z+Y)\right]_{3,4}$	0.240 ± 0.020	87	Y_1Y_3	0.478 ± 0.011
28	$\left[\frac{1}{\sqrt{2}}(Z+X)\right]_{1,2,3}$	0.385 ± 0.019	58	$\left[\frac{1}{\sqrt{2}}(Z+Y)\right]_{1,2,3}$	0.420 ± 0.019	88	X_2X_4	0.487 ± 0.011
29	$\left[\frac{1}{\sqrt{2}}(Z+X)\right]_{1,2,4}$	0.357 ± 0.019	59	$\left[\frac{1}{\sqrt{2}}(Z+Y)\right]_{1,2,4}$	0.350 ± 0.020	89	Y_2Y_4	0.492 ± 0.011
30	$\left[\frac{1}{\sqrt{2}}(Z+X)\right]_{1,3,4}$	0.339 ± 0.019	60	$\left[\frac{1}{\sqrt{2}}(Z+Y)\right]_{1,3,4}$	0.373 ± 0.019	90	I	1

F_{W_4}	0.971 ± 0.006	
Witnesses	Experimental result	Theoretical expectation(F=1)
$\mathcal{W}_1$	-0.00349 ± 0.00047	-0.0047
$\mathcal{W}_2$	-0.00522 ± 0.00049	-0.0070
$\mathcal{W}_3$	-0.00751 ± 0.00047	-0.0090
$\mathcal{W}_4$	-0.00823 ± 0.00049	-0.0095
$\mathcal{W}_5$	-0.00987 ± 0.00048	-0.0114

TABLE XIV. Experimental results of four-photon W state fidelity and witness under fidelity F = 0.919 ± 0.004. Including the required 90 operator expectation values. Under the conditions of unfiltered parametric light, pump power of entangled source in 1000mw, and direct SPDC source in 1200mw, PPKTP crystal temperature of 70℃, and no walk-off compensation offset, no path difference in BS interference. Data were collected for each basis in 300 s (about 7000 events). Error bars are derived from raw data analysis incorporating Poissonian counting statistics.

	Operators	Expectation value		Operators	Expectation value		Operators	Expectation value
1	Z_1	0.528 ± 0.010	31	$\left[\frac{1}{\sqrt{2}}(Z+X)\right]_{2,3,4}$	0.298 ± 0.011	61	$\left[\frac{1}{\sqrt{2}}(Z+Y)\right]_{2,3,4}$	0.297 ± 0.011
2	Z_2	0.500 ± 0.010	32	$\left[\frac{1}{\sqrt{2}}(Z+X)\right]^{\otimes 4}$	0.395 ± 0.011	62	$\left[\frac{1}{\sqrt{2}}(Z+Y)\right]^{\otimes 4}$	0.412 ± 0.011
3	Z_3	0.528 ± 0.010	33	$\left[\frac{1}{\sqrt{2}}(Z-X)\right]_{1}$	0.392 ± 0.011	63	$\left[\frac{1}{\sqrt{2}}(Z-Y)\right]_{1}$	0.393 ± 0.011
4	Z_4	0.416 ± 0.010	34	$\left[\frac{1}{\sqrt{2}}(Z-X)\right]_{2}$	0.396 ± 0.011	64	$\left[\frac{1}{\sqrt{2}}(Z-Y)\right]_{2}$	0.359 ± 0.011
5	Z_1Z_2	0.057 ± 0.011	35	$\left[\frac{1}{\sqrt{2}}(Z-X)\right]_{3}$	0.379 ± 0.011	65	$\left[\frac{1}{\sqrt{2}}(Z-Y)\right]_{3}$	0.351 ± 0.011
6	Z_1Z_3	0.084 ± 0.011	36	$\left[\frac{1}{\sqrt{2}}(Z-X)\right]_{4}$	0.299 ± 0.011	66	$\left[\frac{1}{\sqrt{2}}(Z-Y)\right]_{4}$	0.337 ± 0.011
7	Z_1Z_4	-0.044 ± 0.011	37	$\left[\frac{1}{\sqrt{2}}(Z-X)\right]_{1,2}$	0.263 ± 0.011	67	$\left[\frac{1}{\sqrt{2}}(Z-Y)\right]_{1,2}$	0.259 ± 0.011
8	Z_2Z_3	0.055 ± 0.011	38	$\left[\frac{1}{\sqrt{2}}(Z-X)\right]_{1,3}$	0.270 ± 0.011	68	$\left[\frac{1}{\sqrt{2}}(Z-Y)\right]_{1,3}$	0.257 ± 0.011
9	Z_2Z_4	-0.077 ± 0.011	39	$\left[\frac{1}{\sqrt{2}}(Z-X)\right]_{1,4}$	0.204 ± 0.012	69	$\left[\frac{1}{\sqrt{2}}(Z-Y)\right]_{1,4}$	0.199 ± 0.011
10	Z_3Z_4	-0.051 ± 0.011	40	$\left[\frac{1}{\sqrt{2}}(Z-X)\right]_{2,3}$	0.246 ± 0.011	70	$\left[\frac{1}{\sqrt{2}}(Z-Y)\right]_{2,3}$	0.248 ± 0.011
11	$Z_1Z_2Z_3$	-0.406 ± 0.010	41	$\left[\frac{1}{\sqrt{2}}(Z-X)\right]_{2,4}$	0.218 ± 0.012	71	$\left[\frac{1}{\sqrt{2}}(Z-Y)\right]_{2,4}$	0.217 ± 0.011
12	$Z_1Z_2Z_4$	-0.512 ± 0.010	42	$\left[\frac{1}{\sqrt{2}}(Z-X)\right]_{3,4}$	0.219 ± 0.012	72	$\left[\frac{1}{\sqrt{2}}(Z-Y)\right]_{3,4}$	0.223 ± 0.011
13	$Z_1Z_3Z_4$	-0.486 ± 0.010	43	$\left[\frac{1}{\sqrt{2}}(Z-X)\right]_{1,2,3}$	0.327 ± 0.011	73	$\left[\frac{1}{\sqrt{2}}(Z-Y)\right]_{1,2,3}$	0.332 ± 0.011
14	$Z_2Z_3Z_4$	-0.519 ± 0.010	44	$\left[\frac{1}{\sqrt{2}}(Z-X)\right]_{1,2,4}$	0.297 ± 0.011	74	$\left[\frac{1}{\sqrt{2}}(Z-Y)\right]_{1,2,4}$	0.302 ± 0.011
15	$Z^{\otimes 4}$	-0.975 ± 0.003	45	$\left[\frac{1}{\sqrt{2}}(Z-X)\right]_{1,3,4}$	0.311 ± 0.011	75	$\left[\frac{1}{\sqrt{2}}(Z-Y)\right]_{1,3,4}$	0.295 ± 0.011
16	$X^{\otimes 4}$	0.007 ± 0.012	46	$\left[\frac{1}{\sqrt{2}}(Z-X)\right]_{2,3,4}$	0.296 ± 0.011	76	$\left[\frac{1}{\sqrt{2}}(Z-Y)\right]_{2,3,4}$	0.306 ± 0.011
17	$Y^{\otimes 4}$	-0.008 ± 0.012	47	$\left[\frac{1}{\sqrt{2}}(Z-X)\right]^{\otimes 4}$	0.413 ± 0.011	77	$\left[\frac{1}{\sqrt{2}}(Z-Y)\right]^{\otimes 4}$	0.429 ± 0.011
18	$\left[\frac{1}{\sqrt{2}}(Z+X)\right]_{1}$	0.363 ± 0.011	48	$\left[\frac{1}{\sqrt{2}}(Z+Y)\right]_{1}$	0.390 ± 0.011	78	X_1X_2	0.407 ± 0.011
19	$\left[\frac{1}{\sqrt{2}}(Z+X)\right]_{2}$	0.367 ± 0.011	49	$\left[\frac{1}{\sqrt{2}}(Z+Y)\right]_{2}$	0.363 ± 0.011	79	Y_1Y_2	0.392 ± 0.011
20	$\left[\frac{1}{\sqrt{2}}(Z+X)\right]_{3}$	0.372 ± 0.011	50	$\left[\frac{1}{\sqrt{2}}(Z+Y)\right]_{3}$	0.395 ± 0.011	80	X_2X_3	0.437 ± 0.011
21	$\left[\frac{1}{\sqrt{2}}(Z+X)\right]_{4}$	0.294 ± 0.011	51	$\left[\frac{1}{\sqrt{2}}(Z+Y)\right]_{4}$	0.321 ± 0.011	81	Y_2Y_3	0.416 ± 0.011
22	$\left[\frac{1}{\sqrt{2}}(Z+X)\right]_{1,2}$	0.258 ± 0.011	52	$\left[\frac{1}{\sqrt{2}}(Z+Y)\right]_{1,2}$	0.250 ± 0.011	82	X_3X_4	0.497 ± 0.010
23	$\left[\frac{1}{\sqrt{2}}(Z+X)\right]_{1,3}$	0.249 ± 0.011	53	$\left[\frac{1}{\sqrt{2}}(Z+Y)\right]_{1,3}$	0.257 ± 0.011	83	Y_3Y_4	0.498 ± 0.010
24	$\left[\frac{1}{\sqrt{2}}(Z+X)\right]_{1,4}$	0.179 ± 0.011	54	$\left[\frac{1}{\sqrt{2}}(Z+Y)\right]_{1,4}$	0.227 ± 0.011	84	X_1X_4	0.432 ± 0.011
25	$\left[\frac{1}{\sqrt{2}}(Z+X)\right]_{2,3}$	0.246 ± 0.011	55	$\left[\frac{1}{\sqrt{2}}(Z+Y)\right]_{2,3}$	0.247 ± 0.011	85	Y_1Y_4	0.409 ± 0.011
26	$\left[\frac{1}{\sqrt{2}}(Z+X)\right]_{2,4}$	0.207 ± 0.011	56	$\left[\frac{1}{\sqrt{2}}(Z+Y)\right]_{2,4}$	0.220 ± 0.011	86	X_1X_3	0.430 ± 0.011
27	$\left[\frac{1}{\sqrt{2}}(Z+X)\right]_{3,4}$	0.185 ± 0.011	57	$\left[\frac{1}{\sqrt{2}}(Z+Y)\right]_{3,4}$	0.212 ± 0.011	87	Y_1Y_3	0.417 ± 0.011
28	$\left[\frac{1}{\sqrt{2}}(Z+X)\right]_{1,2,3}$	0.304 ± 0.011	58	$\left[\frac{1}{\sqrt{2}}(Z+Y)\right]_{1,2,3}$	0.312 ± 0.011	88	X_2X_4	0.488 ± 0.010
29	$\left[\frac{1}{\sqrt{2}}(Z+X)\right]_{1,2,4}$	0.288 ± 0.011	59	$\left[\frac{1}{\sqrt{2}}(Z+Y)\right]_{1,2,4}$	0.307 ± 0.011	89	Y_2Y_4	0.474 ± 0.010
30	$\left[\frac{1}{\sqrt{2}}(Z+X)\right]_{1,3,4}$	0.259 ± 0.011	60	$\left[\frac{1}{\sqrt{2}}(Z+Y)\right]_{1,3,4}$	0.304 ± 0.011	90	I	1

F_{W_4}	0.919 ± 0.004	
Witnesses	Experimental result	Theoretical expectation(F=1)
$\mathcal{W}_1$	0.000184 ± 0.000451	-0.0047
$\mathcal{W}_2$	-0.00153 ± 0.00047	-0.0070
$\mathcal{W}_3$	-0.00351 ± 0.00045	-0.0090
$\mathcal{W}_4$	-0.00416 ± 0.00047	-0.0095
$\mathcal{W}_5$	-0.00619 ± 0.00045	-0.0114

TABLE XV. Experimental results of four-photon W state fidelity and witness under fidelity F = 0.720 ± 0.004. Including the required 90 operator expectation values. Under the conditions of unfiltered parametric light, pump power of entangled source in 1000mw, and direct SPDC source in 1000mw, PPKTP crystal temperature of 70℃, and walk-off compensation no offset, 40μm path difference in BS interference. Data were collected for each basis in 300 s (about 8000 events). Error bars are derived from raw data analysis incorporating Poissonian counting statistics.

	Operators	Expectation value		Operators	Expectation value		Operators	Expectation value
1	Z_1	0.587 ± 0.009	31	$\left[\frac{1}{\sqrt{2}}(Z+X)\right]_{2,3,4}$	0.211 ± 0.011	61	$\left[\frac{1}{\sqrt{2}}(Z+Y)\right]_{2,3,4}$	0.194 ± 0.011
2	Z_2	0.526 ± 0.009	32	$\left[\frac{1}{\sqrt{2}}(Z+X)\right]^{\otimes 4}$	0.261 ± 0.011	62	$\left[\frac{1}{\sqrt{2}}(Z+Y)\right]^{\otimes 4}$	0.227 ± 0.011
3	Z_3	0.557 ± 0.009	33	$\left[\frac{1}{\sqrt{2}}(Z-X)\right]_{1}$	0.438 ± 0.010	63	$\left[\frac{1}{\sqrt{2}}(Z-Y)\right]_{1}$	0.405 ± 0.010
4	Z_4	0.306 ± 0.010	34	$\left[\frac{1}{\sqrt{2}}(Z-X)\right]_{2}$	0.432 ± 0.010	64	$\left[\frac{1}{\sqrt{2}}(Z-Y)\right]_{2}$	0.408 ± 0.010
5	Z_1Z_2	0.132 ± 0.011	35	$\left[\frac{1}{\sqrt{2}}(Z-X)\right]_{3}$	0.404 ± 0.010	65	$\left[\frac{1}{\sqrt{2}}(Z-Y)\right]_{3}$	0.404 ± 0.010
6	Z_1Z_3	0.166 ± 0.011	36	$\left[\frac{1}{\sqrt{2}}(Z-X)\right]_{4}$	0.218 ± 0.011	66	$\left[\frac{1}{\sqrt{2}}(Z-Y)\right]_{4}$	0.253 ± 0.011
7	Z_1Z_4	-0.100 ± 0.011	37	$\left[\frac{1}{\sqrt{2}}(Z-X)\right]_{1,2}$	0.235 ± 0.011	67	$\left[\frac{1}{\sqrt{2}}(Z-Y)\right]_{1,2}$	0.220 ± 0.011
8	Z_2Z_3	0.105 ± 0.011	38	$\left[\frac{1}{\sqrt{2}}(Z-X)\right]_{1,3}$	0.228 ± 0.011	68	$\left[\frac{1}{\sqrt{2}}(Z-Y)\right]_{1,3}$	0.236 ± 0.011
9	Z_2Z_4	-0.162 ± 0.011	39	$\left[\frac{1}{\sqrt{2}}(Z-X)\right]_{1,4}$	-0.036 ± 0.011	69	$\left[\frac{1}{\sqrt{2}}(Z-Y)\right]_{1,4}$	-0.026 ± 0.011
10	Z_3Z_4	-0.126 ± 0.011	40	$\left[\frac{1}{\sqrt{2}}(Z-X)\right]_{2,3}$	0.249 ± 0.011	70	$\left[\frac{1}{\sqrt{2}}(Z-Y)\right]_{2,3}$	0.221 ± 0.011
11	$Z_1Z_2Z_3$	-0.296 ± 0.010	41	$\left[\frac{1}{\sqrt{2}}(Z-X)\right]_{2,4}$	0.114 ± 0.011	71	$\left[\frac{1}{\sqrt{2}}(Z-Y)\right]_{2,4}$	0.131 ± 0.011
12	$Z_1Z_2Z_4$	-0.551 ± 0.009	42	$\left[\frac{1}{\sqrt{2}}(Z-X)\right]_{3,4}$	0.135 ± 0.011	72	$\left[\frac{1}{\sqrt{2}}(Z-Y)\right]_{3,4}$	0.119 ± 0.011
13	$Z_1Z_3Z_4$	-0.516 ± 0.009	43	$\left[\frac{1}{\sqrt{2}}(Z-X)\right]_{1,2,3}$	0.210 ± 0.011	73	$\left[\frac{1}{\sqrt{2}}(Z-Y)\right]_{1,2,3}$	0.210 ± 0.011
14	$Z_2Z_3Z_4$	-0.574 ± 0.009	44	$\left[\frac{1}{\sqrt{2}}(Z-X)\right]_{1,2,4}$	0.050 ± 0.011	74	$\left[\frac{1}{\sqrt{2}}(Z-Y)\right]_{1,2,4}$	0.057 ± 0.011
15	$Z^{\otimes 4}$	-0.976 ± 0.002	45	$\left[\frac{1}{\sqrt{2}}(Z-X)\right]_{1,3,4}$	0.076 ± 0.011	75	$\left[\frac{1}{\sqrt{2}}(Z-Y)\right]_{1,3,4}$	0.066 ± 0.011
16	$X^{\otimes 4}$	0.017 ± 0.011	46	$\left[\frac{1}{\sqrt{2}}(Z-X)\right]_{2,3,4}$	0.158 ± 0.011	76	$\left[\frac{1}{\sqrt{2}}(Z-Y)\right]_{2,3,4}$	0.155 ± 0.011
17	$Y^{\otimes 4}$	0.020 ± 0.011	47	$\left[\frac{1}{\sqrt{2}}(Z-X)\right]^{\otimes 4}$	0.162 ± 0.011	77	$\left[\frac{1}{\sqrt{2}}(Z-Y)\right]^{\otimes 4}$	0.164 ± 0.011
18	$\left[\frac{1}{\sqrt{2}}(Z+X)\right]_{1}$	0.398 ± 0.011	48	$\left[\frac{1}{\sqrt{2}}(Z+Y)\right]_{1}$	0.438 ± 0.010	78	X_1X_2	0.307 ± 0.011
19	$\left[\frac{1}{\sqrt{2}}(Z+X)\right]_{2}$	0.383 ± 0.011	49	$\left[\frac{1}{\sqrt{2}}(Z+Y)\right]_{2}$	0.404 ± 0.010	79	Y_1Y_2	0.302 ± 0.011
20	$\left[\frac{1}{\sqrt{2}}(Z+X)\right]_{3}$	0.405 ± 0.011	50	$\left[\frac{1}{\sqrt{2}}(Z+Y)\right]_{3}$	0.423 ± 0.010	80	X_2X_3	0.313 ± 0.011
21	$\left[\frac{1}{\sqrt{2}}(Z+X)\right]_{4}$	0.290 ± 0.011	51	$\left[\frac{1}{\sqrt{2}}(Z+Y)\right]_{4}$	0.250 ± 0.011	81	Y_2Y_3	0.323 ± 0.011
22	$\left[\frac{1}{\sqrt{2}}(Z+X)\right]_{1,2}$	0.248 ± 0.011	52	$\left[\frac{1}{\sqrt{2}}(Z+Y)\right]_{1,2}$	0.261 ± 0.011	82	X_3X_4	0.399 ± 0.010
23	$\left[\frac{1}{\sqrt{2}}(Z+X)\right]_{1,3}$	0.263 ± 0.011	53	$\left[\frac{1}{\sqrt{2}}(Z+Y)\right]_{1,3}$	0.257 ± 0.011	83	Y_3Y_4	0.389 ± 0.011
24	$\left[\frac{1}{\sqrt{2}}(Z+X)\right]_{1,4}$	0.072 ± 0.011	54	$\left[\frac{1}{\sqrt{2}}(Z+Y)\right]_{1,4}$	0.046 ± 0.011	84	X_1X_4	0.141 ± 0.011
25	$\left[\frac{1}{\sqrt{2}}(Z+X)\right]_{2,3}$	0.249 ± 0.011	55	$\left[\frac{1}{\sqrt{2}}(Z+Y)\right]_{2,3}$	0.263 ± 0.011	85	Y_1Y_4	0.155 ± 0.011
26	$\left[\frac{1}{\sqrt{2}}(Z+X)\right]_{2,4}$	0.151 ± 0.011	56	$\left[\frac{1}{\sqrt{2}}(Z+Y)\right]_{2,4}$	0.141 ± 0.011	86	X_1X_3	0.278 ± 0.011
27	$\left[\frac{1}{\sqrt{2}}(Z+X)\right]_{3,4}$	0.142 ± 0.011	57	$\left[\frac{1}{\sqrt{2}}(Z+Y)\right]_{3,4}$	0.127 ± 0.011	87	Y_1Y_3	0.319 ± 0.011
28	$\left[\frac{1}{\sqrt{2}}(Z+X)\right]_{1,2,3}$	0.271 ± 0.011	58	$\left[\frac{1}{\sqrt{2}}(Z+Y)\right]_{1,2,3}$	0.260 ± 0.011	88	X_2X_4	0.399 ± 0.010
29	$\left[\frac{1}{\sqrt{2}}(Z+X)\right]_{1,2,4}$	0.151 ± 0.011	59	$\left[\frac{1}{\sqrt{2}}(Z+Y)\right]_{1,2,4}$	0.147 ± 0.011	89	Y_2Y_4	0.408 ± 0.010
30	$\left[\frac{1}{\sqrt{2}}(Z+X)\right]_{1,3,4}$	0.152 ± 0.011	60	$\left[\frac{1}{\sqrt{2}}(Z+Y)\right]_{1,3,4}$	0.103 ± 0.011	90	I	1

F_{W_4}	0.720 ± 0.004	
Witnesses	Experimental result	Theoretical expectation(F=1)
$\mathcal{W}_1$	0.00830 ± 0.00045	-0.0047
$\mathcal{W}_2$	0.00547 ± 0.00046	-0.0070
$\mathcal{W}_3$	0.00759 ± 0.00044	-0.0090
$\mathcal{W}_4$	0.00698 ± 0.00046	-0.0095
$\mathcal{W}_5$	0.00379 ± 0.00043	-0.0114

5. Four Photon Cluster State

The the detailed configurations are shown in Tables XVI, and results for measuring the fidelity and witness of the four-photon cluster state are presented in Tables XVII and XVIII.

TABLE XVI. Experimental configurations of four-photon Cluster state.

Fidelity	0.968 ± 0.002	0.880 ± 0.003
Spectral filtering	1550 ± 10 nm	unfiltered
Pump Laser Power of entangled source	240 mW	1100 mW
Pump Laser Power of direct SPDC	240 mW	1100 mW
PPKTP crystal temperature (both)	25°C	25°C
interference optical range difference	0	0
Rate of counting	0.70/s	68/s

TABLE XVII. Experimental results of four-photon Cluster state fidelity and witness under fidelity F = 0.968 ± 0.002. Including the required 16 operator expectation values. Under the conditions of 1550±10nm filtered parametric light, pump power of the two entangled source in 240mw, PPKTP crystal temperature of 25℃, no path difference in PDBS interference. Data were collected for each basis in 2100 s (about 1500 events). Error bars are derived from raw data analysis incorporating Poissonian counting statistics.

	Operators	Expectation value		Operators	Expectation
1	Z_1Z_2	0.991 ± 0.003	9	$X_1X_2Z_4$	0.966 ± 0.007
2	$X_1X_2Z_3$	0.967 ± 0.007	10	$Z_2Y_3Y_4$	0.956 ± 0.008
3	$Z_2X_3X_4$	0.956 ± 0.008	11	$Y_1X_2Y_3X_4$	0.946 ± 0.009
4	Z_3Z_4	0.996 ± 0.002	12	$Y_1Y_2Z_4$	0.963 ± 0.007
5	$Y_1Y_2Z_3$	0.965 ± 0.007	13	$Z_1Y_3Y_4$	0.957 ± 0.008
6	$Z_1X_3X_4$	0.960 ± 0.007	14	$X_1Y_2X_3Y_4$	0.958 ± 0.008
7	$Z_1Z_2Z_3Z_4$	0.990 ± 0.004	15	$Y_1X_2X_3Y_4$	0.953 ± 0.008
8	$X_1Y_2Y_3X_4$	0.962 ± 0.007	16	I	1
F_{C_4}		0.968 ± 0.002			
Witnesses		Experimental results	Theoretical expectation(F=1)		
$\mathcal{W}_1$		-0.0132 $\pm$ 0.0002	-0.0156		
$\mathcal{W}_2$		-0.0287 $\pm$ 0.0002	-0.0312		
$\mathcal{W}_3$		-0.0378 $\pm$ 0.0003	-0.0417		
$\mathcal{W}_4$		-0.0573 $\pm$ 0.0003	-0.0625		

TABLE XVIII. Experimental results of four-photon Cluster state fidelity and witness under fidelity F = 0.880 ± 0.003. Including the required 16 operator expectation values. Under the conditions of 1550±10nm filtered parametric light, pump power of the two entangled source in 240mw, PPKTP crystal temperature of 25℃, no path difference in PDBS interference. Data are collected for each basis in 2100 s (about 1500 events). Error bars are derived from raw data analysis incorporating Poissonian counting statistics.

	Operators	Expectation value		Operators	Expectation
1	Z_1Z_2	0.969 ± 0.006	9	$X_1X_2Z_4$	0.859 ± 0.013
2	$X_1X_2Z_3$	0.860 ± 0.013	10	$Z_2Y_3Y_4$	0.857 ± 0.013
3	$Z_2X_3X_4$	0.868 ± 0.012	11	$Y_1X_2Y_3X_4$	0.844 ± 0.013
4	Z_3Z_4	0.982 ± 0.005	12	$Y_1Y_2Z_4$	0.815 ± 0.014
5	$Y_1Y_2Z_3$	0.820 ± 0.014	13	$Z_1Y_3Y_4$	0.840 ± 0.013
6	$Z_1X_3X_4$	0.859 ± 0.013	14	$X_1Y_2X_3Y_4$	0.865 ± 0.012
7	$Z_1Z_2Z_3Z_4$	0.951 ± 0.007	15	$Y_1X_2X_3Y_4$	0.858 ± 0.013
8	$X_1Y_2Y_3X_4$	0.839 ± 0.013	16	I	1
F_{C_4}		0.880 ± 0.003			
Witnesses		Experimental results		Theoretical expectation(F=1)	
$\mathcal{W}_1$		-0.0056 ± 0.0004		-0.0156	
$\mathcal{W}_2$		-0.0207 ± 0.0004		-0.0312	
$\mathcal{W}_3$		-0.0268 ± 0.0005		-0.0417	
$\mathcal{W}_4$		-0.0419 ± 0.0006		-0.0625	

6. Robustness Verification

To verify the robustness of the EDL framework against measurement noise, we demonstrate three deflection angles under two conditions: (a) measurement noise acts on the basis X, Y, and Z, and (b) measurement noise acts solely on the basis Y. The positions of the points collected in our experiment within the theoretically predicted images are shown in Figures 7(a) and (b).

The specific experimental configurations are shown in Tables XIX and XXVI. Detailed results including initial state and noise introdued state in different θ of condition (a) are shown in Tables XX, XXI, XXII, XXIII, XXIV, and XXV, while condition (b) are shown in Tables XXVII, XXVIII, XXIX, XXX, XXXI, and XXXII.

TABLE XIX. Experimental configurations of robustness verification based on four-photon Dicke state (noise introduced on basis X, Y, and Z).

condition	$\theta = 2\pi/15$	$\theta = \pi/8$	$\theta = \pi/9$
Fidelity(original)	0.925 ± 0.003	0.894 ± 0.003	0.849 ± 0.003
Fidelity(noise introduced)	0.611 ± 0.004	0.603 ± 0.004	0.645 ± 0.004
Spectral filtering	unfiltered	unfiltered	unfiltered
Pump Laser Power	1350 mW	3100 mW	3100 mW
PPKTP crystal temperature	17°C	17°C	50°C
Walk-off compensation	No offset	No offset	No offset
Rate of counting	18.5/s	98/s	98/s

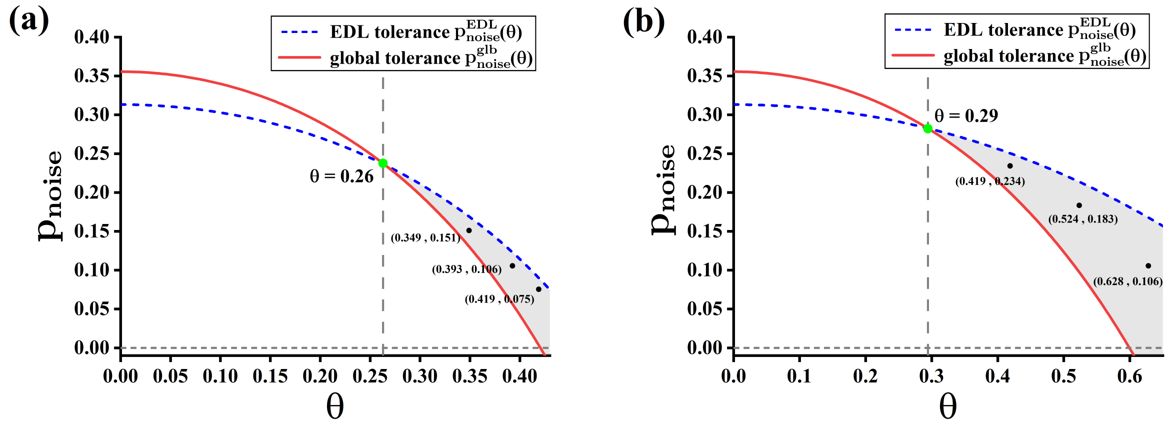

FIG. 7. The position of experimental results on the theoretical image. The horizontal coordinate θ of the data points represents the deflection angle set in the experiment, while the vertical coordinate $p_{\text{noise}} = 1 - F_{\text{D}_4}$ is calculated from the fidelity of the initial state prepared in the experiment. (a) measurement noise acts on the basis X, Y, and Z, (b) measurement noise acts solely on the basis Y.

TABLE XX. Results of fidelity and witness of the initial four-photon Dicke state prepared for robustness verification with noise $\theta = 2\pi/15$. Including the required 27 operator expectation values. Under the conditions of no filtering of the parametric light, pump laser power of 1350mw, PPKTP crystal temperature of 17℃. Data are collected for each basis in 300 s (about 5600 events). Error bars are derived from raw data analysis incorporating Poissonian counting statistics.

Operators		Expectation value	Operators		Expectation value
1	X_1X_2	0.655 ± 0.010	15	Z_1Z_2	-0.357 ± 0.012
2	X_1X_3	0.571 ± 0.011	16	Z_1Z_3	-0.360 ± 0.012
3	X_1X_4	0.572 ± 0.011	17	Z_1Z_4	-0.253 ± 0.013
4	X_2X_3	0.577 ± 0.011	18	Z_2Z_3	-0.250 ± 0.013
5	X_2X_4	0.574 ± 0.011	19	Z_2Z_4	-0.354 ± 0.012
6	X_3X_4	0.661 ± 0.010	20	Z_3Z_4	-0.359 ± 0.012
7	$X_1X_2X_3X_4$	0.945 ± 0.004	21	$Z_1Z_2Z_3Z_4$	0.934 ± 0.005
8	Y_1Y_2	0.682 ± 0.010	22	$[\frac{1}{\sqrt{2}}(X+Z)]^{\otimes 4}$	-0.427 ± 0.012
9	Y_1Y_3	0.586 ± 0.011	23	$[\frac{1}{\sqrt{2}}(X-Z)]^{\otimes 4}$	-0.453 ± 0.012
10	Y_1Y_4	0.592 ± 0.010	24	$[\frac{1}{\sqrt{2}}(Y+Z)]^{\otimes 4}$	-0.434 ± 0.012
11	Y_2Y_3	0.591 ± 0.010	25	$[\frac{1}{\sqrt{2}}(Y-Z)]^{\otimes 4}$	-0.434 ± 0.012
12	Y_2Y_4	0.586 ± 0.011	26	$[\frac{1}{\sqrt{2}}(X+Y)]^{\otimes 4}$	0.936 ± 0.005
13	Y_3Y_4	0.685 ± 0.009	27	$[\frac{1}{\sqrt{2}}(X-Y)]^{\otimes 4}$	0.932 ± 0.005
14	$Y_1Y_2Y_3Y_4$	0.937 ± 0.005	W_{proj}		-0.258 ± 0.003
$F_{\text{D}_4^{(2)}}$		0.925 ± 0.003	W_5		-0.0224 ± 0.0005

TABLE XXI. Results of fidelity and witness of four-photon Dicke state at noise $\theta = 2\pi/15$. Including the required 27 operator expectation values. Under the conditions of no filtering of the parametric light, pump laser power of 1350mw, PPKTP crystal temperature of 17℃. Data are collected for each basis in 300 s (about 5600 events). Error bars are derived from raw data analysis incorporating Poissonian counting statistics.

Operators		Expectation value	Operators		Expectation value
1	X_1X_2	0.661 ± 0.010	15	Z_1Z_2	-0.227 ± 0.013
2	X_1X_3	0.574 ± 0.011	16	Z_1Z_3	-0.185 ± 0.013
3	X_1X_4	0.570 ± 0.011	17	Z_1Z_4	-0.121 ± 0.013
4	X_2X_3	0.568 ± 0.011	18	Z_2Z_3	-0.140 ± 0.013
5	X_2X_4	0.588 ± 0.011	19	Z_2Z_4	-0.194 ± 0.013
6	X_3X_4	0.663 ± 0.010	20	Z_3Z_4	-0.173 ± 0.013
7	$X_1X_2X_3X_4$	0.937 ± 0.005	21	$Z_1Z_2Z_3Z_4$	0.204 ± 0.013
8	Y_1Y_2	0.506 ± 0.011	22	$[\frac{1}{\sqrt{2}}(X+Z)]^{\otimes 4}$	-0.187 ± 0.013
9	Y_1Y_3	0.431 ± 0.012	23	$[\frac{1}{\sqrt{2}}(X-Z)]^{\otimes 4}$	-0.329 ± 0.013
10	Y_1Y_4	0.465 ± 0.012	24	$[\frac{1}{\sqrt{2}}(Y+Z)]^{\otimes 4}$	-0.381 ± 0.012
11	Y_2Y_3	0.462 ± 0.012	25	$[\frac{1}{\sqrt{2}}(Y-Z)]^{\otimes 4}$	-0.009 ± 0.013
12	Y_2Y_4	0.486 ± 0.012	26	$[\frac{1}{\sqrt{2}}(X+Y)]^{\otimes 4}$	0.682 ± 0.010
13	Y_3Y_4	0.543 ± 0.011	27	$[\frac{1}{\sqrt{2}}(X-Y)]^{\otimes 4}$	0.480 ± 0.012
14	$Y_1Y_2Y_3Y_4$	0.280 ± 0.013	$W_{\rm proj}$		0.056 ± 0.004
$F_{\mathrm{D}_4^{(2)}}$		0.611 ± 0.004	W_5		-0.0029 ± 0.0006

TABLE XXII. Results of fidelity and witness of the initial four-photon Dicke state prepared for robustness verification with noise $\theta = \pi/8$. Including the required 27 operator expectation values. Under the conditions of no filtering of the parametric light, pump laser power of 3100mw, PPKTP crystal temperature of 17℃. Data are collected for each basis in 60 s (about 5600 events). Error bars are derived from raw data analysis incorporating Poissonian counting statistics.

Operators		Expectation value	Operators		Expectation value
1	X_1X_2	0.651 ± 0.010	15	Z_1Z_2	-0.346 ± 0.012
2	X_1X_3	0.566 ± 0.011	16	Z_1Z_3	-0.343 ± 0.012
3	X_1X_4	0.564 ± 0.011	17	Z_1Z_4	-0.266 ± 0.012
4	X_2X_3	0.558 ± 0.011	18	Z_2Z_3	-0.267 ± 0.012
5	X_2X_4	0.584 ± 0.011	19	Z_2Z_4	-0.344 ± 0.012
6	X_3X_4	0.647 ± 0.010	20	Z_3Z_4	-0.318 ± 0.012
7	$X_1X_2X_3X_4$	0.892 ± 0.006	21	$Z_1Z_2Z_3Z_4$	0.884 ± 0.006
8	Y_1Y_2	0.664 ± 0.010	22	$[\frac{1}{\sqrt{2}}(X+Z)]^{\otimes 4}$	-0.424 ± 0.012
9	Y_1Y_3	0.596 ± 0.011	23	$[\frac{1}{\sqrt{2}}(X-Z)]^{\otimes 4}$	-0.399 ± 0.012
10	Y_1Y_4	0.599 ± 0.011	24	$[\frac{1}{\sqrt{2}}(Y+Z)]^{\otimes 4}$	-0.401 ± 0.012
11	Y_2Y_3	0.598 ± 0.011	25	$[\frac{1}{\sqrt{2}}(Y-Z)]^{\otimes 4}$	-0.397 ± 0.012
12	Y_2Y_4	0.595 ± 0.011	26	$[\frac{1}{\sqrt{2}}(X+Y)]^{\otimes 4}$	0.888 ± 0.006
13	Y_3Y_4	0.668 ± 0.010	27	$[\frac{1}{\sqrt{2}}(X-Y)]^{\otimes 4}$	0.916 ± 0.005
14	$Y_1Y_2Y_3Y_4$	0.906 ± 0.006	$W_{\rm proj}$		-0.228 ± 0.003
$F_{\mathrm{D}_4^{(2)}}$		0.894 ± 0.003	W_5		-0.0213 ± 0.0005

TABLE XXIII. Results of verify the fidelity and witness of four-photon Dicke state at noise $\theta = \pi/8$. Including the required 27 operator expectation values. Under the conditions of no filtering of the parametric light, pump laser power of 3100mw, PPKTP crystal temperature of 17℃. Data are collected for each basis in 60 s (about 5600 events). Error bars are derived from raw data analysis incorporating Poissonian counting statistics.

Operators		Expectation value	Operators		Expectation value
1	X_1X_2	0.670 ± 0.010	15	Z_1Z_2	-0.197 ± 0.013
2	X_1X_3	0.583 ± 0.011	16	Z_1Z_3	-0.162 ± 0.013
3	X_1X_4	0.592 ± 0.011	17	Z_1Z_4	-0.149 ± 0.013
4	X_2X_3	0.591 ± 0.011	18	Z_2Z_3	-0.122 ± 0.013
5	X_2X_4	0.609 ± 0.010	19	Z_2Z_4	-0.207 ± 0.013
6	X_3X_4	0.662 ± 0.010	20	Z_3Z_4	-0.152 ± 0.013
7	$X_1X_2X_3X_4$	0.897 ± 0.006	21	$Z_1Z_2Z_3Z_4$	0.171 ± 0.013
8	Y_1Y_2	0.540 ± 0.011	22	$[\frac{1}{\sqrt{2}}(X+Z)]^{\otimes 4}$	-0.154 ± 0.013
9	Y_1Y_3	0.473 ± 0.011	23	$[\frac{1}{\sqrt{2}}(X-Z)]^{\otimes 4}$	-0.217 ± 0.013
10	Y_1Y_4	0.478 ± 0.011	24	$[\frac{1}{\sqrt{2}}(Y+Z)]^{\otimes 4}$	-0.362 ± 0.012
11	Y_2Y_3	0.489 ± 0.011	25	$[\frac{1}{\sqrt{2}}(Y-Z)]^{\otimes 4}$	-0.022 ± 0.013
12	Y_2Y_4	0.506 ± 0.011	26	$[\frac{1}{\sqrt{2}}(X+Y)]^{\otimes 4}$	0.747 ± 0.009
13	Y_3Y_4	0.530 ± 0.011	27	$[\frac{1}{\sqrt{2}}(X-Y)]^{\otimes 4}$	0.388 ± 0.012
14	$Y_1Y_2Y_3Y_4$	0.360 ± 0.012	W_{proj}		0.064 ± 0.004
$F_{\text{D}_4^{(2)}}$		0.603 ± 0.004	W_5		-0.0037 ± 0.0006

TABLE XXIV. Results of fidelity and witness of the initial four-photon Dicke state prepared for robustness verification with noise $\theta = \pi/9$. Including the required 27 operator expectation values. Under the conditions of no filtering of the parametric light, pump laser power of 3100mw, PPKTP crystal temperature of 50℃. Data are collected for each basis in 60 s (about 5600 events). Error bars are derived from raw data analysis incorporating Poissonian counting statistics.

Operators		Expectation value	Operators		Expectation value
1	X_1X_2	0.618 ± 0.010	15	Z_1Z_2	-0.342 ± 0.012
2	X_1X_3	0.554 ± 0.011	16	Z_1Z_3	-0.349 ± 0.012
3	X_1X_4	0.543 ± 0.011	17	Z_1Z_4	-0.256 ± 0.012
4	X_2X_3	0.548 ± 0.011	18	Z_2Z_3	-0.255 ± 0.012
5	X_2X_4	0.560 ± 0.011	19	Z_2Z_4	-0.349 ± 0.012
6	X_3X_4	0.612 ± 0.010	20	Z_3Z_4	-0.333 ± 0.012
7	$X_1X_2X_3X_4$	0.805 ± 0.008	21	$Z_1Z_2Z_3Z_4$	0.886 ± 0.006
8	Y_1Y_2	0.643 ± 0.010	22	$[\frac{1}{\sqrt{2}}(X+Z)]^{\otimes 4}$	-0.385 ± 0.012
9	Y_1Y_3	0.560 ± 0.011	23	$[\frac{1}{\sqrt{2}}(X-Z)]^{\otimes 4}$	-0.373 ± 0.012
10	Y_1Y_4	0.551 ± 0.011	24	$[\frac{1}{\sqrt{2}}(Y+Z)]^{\otimes 4}$	-0.377 ± 0.012
11	Y_2Y_3	0.553 ± 0.011	25	$[\frac{1}{\sqrt{2}}(Y-Z)]^{\otimes 4}$	-0.381 ± 0.012
12	Y_2Y_4	0.565 ± 0.011	26	$[\frac{1}{\sqrt{2}}(X+Y)]^{\otimes 4}$	0.801 ± 0.008
13	Y_3Y_4	0.649 ± 0.010	27	$[\frac{1}{\sqrt{2}}(X-Y)]^{\otimes 4}$	0.803 ± 0.008
14	$Y_1Y_2Y_3Y_4$	0.814 ± 0.008	W_{proj}		-0.182 ± 0.003
$F_{\text{D}_4^{(2)}}$		0.849 ± 0.003	W_5		-0.0188 ± 0.0005

TABLE XXV. Results of verify the fidelity and witness of four-photon Dicke state at noise $\theta = \pi/9$. Including the required 27 operator expectation values. Under the conditions of no filtering of the parametric light, pump laser power of 3100mw, PPKTP crystal temperature of 50℃. Data are collected for each basis in 60 s (about 5600 events). Error bars are derived from raw data analysis incorporating Poissonian counting statistics.

Operators		Expectation value	Operators		Expectation value
1	X_1X_2	0.630 ± 0.010	15	Z_1Z_2	-0.253 ± 0.013
2	X_1X_3	0.552 ± 0.011	16	Z_1Z_3	-0.218 ± 0.013
3	X_1X_4	0.547 ± 0.011	17	Z_1Z_4	-0.160 ± 0.013
4	X_2X_3	0.549 ± 0.011	18	Z_2Z_3	-0.160 ± 0.013
5	X_2X_4	0.559 ± 0.011	19	Z_2Z_4	-0.251 ± 0.013
6	X_3X_4	0.631 ± 0.010	20	Z_3Z_4	-0.222 ± 0.013
7	$X_1X_2X_3X_4$	0.804 ± 0.008	21	$Z_1Z_2Z_3Z_4$	0.364 ± 0.012
8	Y_1Y_2	0.552 ± 0.011	22	$[\frac{1}{\sqrt{2}}(X+Z)]^{\otimes 4}$	-0.246 ± 0.013
9	Y_1Y_3	0.473 ± 0.012	23	$[\frac{1}{\sqrt{2}}(X-Z)]^{\otimes 4}$	-0.255 ± 0.013
10	Y_1Y_4	0.479 ± 0.012	24	$[\frac{1}{\sqrt{2}}(Y+Z)]^{\otimes 4}$	-0.339 ± 0.012
11	Y_2Y_3	0.497 ± 0.011	25	$[\frac{1}{\sqrt{2}}(Y-Z)]^{\otimes 4}$	-0.171 ± 0.013
12	Y_2Y_4	0.505 ± 0.011	26	$[\frac{1}{\sqrt{2}}(X+Y)]^{\otimes 4}$	0.665 ± 0.010
13	Y_3Y_4	0.556 ± 0.011	27	$[\frac{1}{\sqrt{2}}(X-Y)]^{\otimes 4}$	0.462 ± 0.011
14	$Y_1Y_2Y_3Y_4$	0.391 ± 0.012	W_{proj}		0.022 ± 0.004
$F_{\text{D}_4^{(2)}}$		0.645 ± 0.004	W_5		-0.0063 ± 0.0006

TABLE XXVI. Experimental configurations of robustness verification based on four-photon Dicke state (noise introduced only on basis Y).

condition	$\theta = \pi/5$	$\theta = \pi/6$	$2\pi/15$
Fidelity(original)	0.894 ± 0.003	0.817 ± 0.003	0.766 ± 0.003
Fidelity(noise introduced)	0.613 ± 0.003	0.620 ± 0.003	0.650 ± 0.003
spectral filtering	unfiltered	unfiltered	unfiltered
Pump Laser Power	3100 mW	3100 mW	3100 mW
PPKTP crystal temperature	17°C	60°C	70°C
Walk-off compensation	No offset	No offset	No offset
Rate of counting	98/s	98/s	101/s

TABLE XXVII. Results of fidelity and witness of the initial four-photon Dicke state prepared for robustness verification with noise $\theta = \pi/5$. Including the required 27 operator expectation values. Under the conditions of no filtering of the parametric light, pump laser power of 3100mw, PPKTP crystal temperature of 17℃(the same condition as XXII). Data are collected for each basis in 60 s (about 5600 events). Error bars are derived from raw data analysis incorporating Poissonian counting statistics.

Operators		Expectation value	Operators		Expectation value
1	X_1X_2	0.651 ± 0.010	15	Z_1Z_2	-0.346 ± 0.012
2	X_1X_3	0.566 ± 0.011	16	Z_1Z_3	-0.343 ± 0.012
3	X_1X_4	0.564 ± 0.011	17	Z_1Z_4	-0.266 ± 0.012
4	X_2X_3	0.558 ± 0.011	18	Z_2Z_3	-0.267 ± 0.012
5	X_2X_4	0.584 ± 0.011	19	Z_2Z_4	-0.344 ± 0.012
6	X_3X_4	0.647 ± 0.010	20	Z_3Z_4	-0.318 ± 0.012
7	$X_1X_2X_3X_4$	0.892 ± 0.006	21	$Z_1Z_2Z_3Z_4$	0.884 ± 0.006
8	Y_1Y_2	0.664 ± 0.010	22	$[\frac{1}{\sqrt{2}}(X+Z)]^{\otimes 4}$	-0.424 ± 0.012
9	Y_1Y_3	0.596 ± 0.011	23	$[\frac{1}{\sqrt{2}}(X-Z)]^{\otimes 4}$	-0.399 ± 0.012
10	Y_1Y_4	0.599 ± 0.011	24	$[\frac{1}{\sqrt{2}}(Y+Z)]^{\otimes 4}$	-0.401 ± 0.012
11	Y_2Y_3	0.598 ± 0.011	25	$[\frac{1}{\sqrt{2}}(Y-Z)]^{\otimes 4}$	-0.397 ± 0.012
12	Y_2Y_4	0.595 ± 0.011	26	$[\frac{1}{\sqrt{2}}(X+Y)]^{\otimes 4}$	0.888 ± 0.006
13	Y_3Y_4	0.668 ± 0.010	27	$[\frac{1}{\sqrt{2}}(X-Y)]^{\otimes 4}$	0.916 ± 0.005
14	$Y_1Y_2Y_3Y_4$	0.906 ± 0.006	W_{proj}		-0.228 ± 0.003
$F_{\mathrm{D}_4^{(2)}}$		0.894 ± 0.003	W_5		-0.0213 ± 0.0005

TABLE XXVIII. Results of fidelity and witness of four-photon Dicke state at noise $\theta = 2\pi/15$. Including the required 27 operator expectation values. Under the conditions of no filtering of the parametric light, pump laser power of 3100mw, PPKTP crystal temperature of 17℃. Data are collected for each basis in 60 s (about 5600 events). Error bars are derived from raw data analysis incorporating Poissonian counting statistics.

Operators		Expectation value	Operators		Expectation value
1	X_1X_2	0.652 ± 0.010	15	Z_1Z_2	-0.342 ± 0.012
2	X_1X_3	0.574 ± 0.011	16	Z_1Z_3	-0.349 ± 0.012
3	X_1X_4	0.592 ± 0.011	17	Z_1Z_4	-0.254 ± 0.013
4	X_2X_3	0.595 ± 0.011	18	Z_2Z_3	-0.248 ± 0.013
5	X_2X_4	0.592 ± 0.011	19	Z_2Z_4	-0.356 ± 0.012
6	X_3X_4	0.654 ± 0.010	20	Z_3Z_4	-0.331 ± 0.012
7	$X_1X_2X_3X_4$	0.902 ± 0.006	21	$Z_1Z_2Z_3Z_4$	0.886 ± 0.006
8	Y_1Y_2	0.340 ± 0.012	22	$[\frac{1}{\sqrt{2}}(X+Z)]^{\otimes 4}$	-0.398 ± 0.012
9	Y_1Y_3	0.303 ± 0.012	23	$[\frac{1}{\sqrt{2}}(X-Z)]^{\otimes 4}$	-0.418 ± 0.012
10	Y_1Y_4	0.322 ± 0.012	24	$[\frac{1}{\sqrt{2}}(Y+Z)]^{\otimes 4}$	-0.041 ± 0.013
11	Y_2Y_3	0.323 ± 0.012	25	$[\frac{1}{\sqrt{2}}(Y-Z)]^{\otimes 4}$	0.009 ± 0.013
12	Y_2Y_4	0.321 ± 0.012	26	$[\frac{1}{\sqrt{2}}(X+Y)]^{\otimes 4}$	0.276 ± 0.013
13	Y_3Y_4	0.364 ± 0.012	27	$[\frac{1}{\sqrt{2}}(X-Y)]^{\otimes 4}$	0.189 ± 0.013
14	$Y_1Y_2Y_3Y_4$	-0.207 ± 0.013	W_{proj}		0.053 ± 0.003
$F_{D_4^{(2)}}$		0.613 ± 0.003	W_5		-0.0085 ± 0.0005

TABLE XXIX. Results of fidelity and witness of the initial four-photon Dicke state prepared for robustness verification with noise $\theta = \pi/6$. Including the required 27 operator expectation values. Under the conditions of no filtering of the parametric light, pump laser power of 3100mw, PPKTP crystal temperature of 60℃. Data are collected for each basis in 60 s (about 5900 events). Error bars are derived from raw data analysis incorporating Poissonian counting statistics.

Operators		Expectation value	Operators		Expectation value
1	X_1X_2	0.613 ± 0.010	15	Z_1Z_2	-0.337 ± 0.012
2	X_1X_3	0.530 ± 0.011	16	Z_1Z_3	-0.356 ± 0.012
3	X_1X_4	0.539 ± 0.011	17	Z_1Z_4	-0.266 ± 0.012
4	X_2X_3	0.543 ± 0.011	18	Z_2Z_3	-0.265 ± 0.012
5	X_2X_4	0.538 ± 0.011	19	Z_2Z_4	-0.346 ± 0.012
6	X_3X_4	0.602 ± 0.010	20	Z_3Z_4	-0.328 ± 0.012
7	$X_1X_2X_3X_4$	0.739 ± 0.009	21	$Z_1Z_2Z_3Z_4$	0.898 ± 0.006
8	Y_1Y_2	0.594 ± 0.010	22	$[\frac{1}{\sqrt{2}}(X+Z)]^{\otimes 4}$	-0.379 ± 0.012
9	Y_1Y_3	0.531 ± 0.011	23	$[\frac{1}{\sqrt{2}}(X-Z)]^{\otimes 4}$	-0.372 ± 0.012
10	Y_1Y_4	0.540 ± 0.011	24	$[\frac{1}{\sqrt{2}}(Y+Z)]^{\otimes 4}$	-0.359 ± 0.012
11	Y_2Y_3	0.540 ± 0.011	25	$[\frac{1}{\sqrt{2}}(Y-Z)]^{\otimes 4}$	-0.342 ± 0.012
12	Y_2Y_4	0.539 ± 0.011	26	$[\frac{1}{\sqrt{2}}(X+Y)]^{\otimes 4}$	0.734 ± 0.009
13	Y_3Y_4	0.591 ± 0.010	27	$[\frac{1}{\sqrt{2}}(X-Y)]^{\otimes 4}$	0.717 ± 0.009
14	$Y_1Y_2Y_3Y_4$	0.737 ± 0.009	W_{proj}		-0.150 ± 0.003
$F_{\text{D}_4^{(2)}}$		0.817 ± 0.003	W_5		-0.0170 ± 0.0005

TABLE XXX. Results of fidelity and witness of four-photon Dicke state at noise $\theta = \pi/6$. Including the required 27 operator expectation values. Under the conditions of no filtering of the parametric light, pump laser power of 3100mw, PPKTP crystal temperature of 60℃. Data are collected for each basis in 60 s (about 5900 events). Error bars are derived from raw data analysis incorporating Poissonian counting statistics.

Operators		Expectation value	Operators		Expectation value
1	X_1X_2	0.594 ± 0.010	15	Z_1Z_2	-0.340 ± 0.012
2	X_1X_3	0.523 ± 0.011	16	Z_1Z_3	-0.338 ± 0.012
3	X_1X_4	0.548 ± 0.011	17	Z_1Z_4	-0.271 ± 0.013
4	X_2X_3	0.544 ± 0.011	18	Z_2Z_3	-0.267 ± 0.013
5	X_2X_4	0.538 ± 0.011	19	Z_2Z_4	-0.334 ± 0.012
6	X_3X_4	0.592 ± 0.010	20	Z_3Z_4	-0.335 ± 0.012
7	$X_1X_2X_3X_4$	0.725 ± 0.009	21	$Z_1Z_2Z_3Z_4$	0.888 ± 0.006
8	Y_1Y_2	0.382 ± 0.012	22	$[\frac{1}{\sqrt{2}}(X+Z)]^{\otimes 4}$	-0.366 ± 0.012
9	Y_1Y_3	0.340 ± 0.012	23	$[\frac{1}{\sqrt{2}}(X-Z)]^{\otimes 4}$	-0.366 ± 0.012
10	Y_1Y_4	0.341 ± 0.012	24	$[\frac{1}{\sqrt{2}}(Y+Z)]^{\otimes 4}$	-0.088 ± 0.013
11	Y_2Y_3	0.368 ± 0.012	25	$[\frac{1}{\sqrt{2}}(Y-Z)]^{\otimes 4}$	-0.132 ± 0.013
12	Y_2Y_4	0.358 ± 0.012	26	$[\frac{1}{\sqrt{2}}(X+Y)]^{\otimes 4}$	0.267 ± 0.012
13	Y_3Y_4	0.388 ± 0.012	27	$[\frac{1}{\sqrt{2}}(X-Y)]^{\otimes 4}$	0.300 ± 0.012
14	$Y_1Y_2Y_3Y_4$	-0.051 ± 0.013	W_{proj}		0.046 ± 0.003
$F_{\text{D}_4^{(2)}}$		0.620 ± 0.003	W_5		-0.0077 ± 0.0005

TABLE XXXI. Results of fidelity and witness of the initial four-photon Dicke state prepared for robustness verification with noise $\theta = 2\pi/15$. Including the required 27 operator expectation values. Under the conditions of no filtering of the parametric light, pump laser power of 3100mw, PPKTP crystal temperature of 70℃. Data are collected for each basis in 60 s (about 5600 events). Error bars are derived from raw data analysis incorporating Poissonian counting statistics.

Operators		Expectation value	Operators		Expectation value
1	X_1X_2	0.566 ± 0.011	15	Z_1Z_2	-0.355 ± 0.012
2	X_1X_3	0.495 ± 0.011	16	Z_1Z_3	-0.363 ± 0.012
3	X_1X_4	0.501 ± 0.011	17	Z_1Z_4	-0.240 ± 0.012
4	X_2X_3	0.494 ± 0.011	18	Z_2Z_3	-0.238 ± 0.012
5	X_2X_4	0.500 ± 0.011	19	Z_2Z_4	-0.352 ± 0.012
6	X_3X_4	0.558 ± 0.011	20	Z_3Z_4	-0.340 ± 0.012
7	$X_1X_2X_3X_4$	0.632 ± 0.010	21	$Z_1Z_2Z_3Z_4$	0.891 ± 0.006
8	Y_1Y_2	0.553 ± 0.011	22	$[\frac{1}{\sqrt{2}}(X+Z)]^{\otimes 4}$	-0.345 ± 0.012
9	Y_1Y_3	0.499 ± 0.011	23	$[\frac{1}{\sqrt{2}}(X-Z)]^{\otimes 4}$	-0.352 ± 0.012
10	Y_1Y_4	0.491 ± 0.011	24	$[\frac{1}{\sqrt{2}}(Y+Z)]^{\otimes 4}$	-0.364 ± 0.012
11	Y_2Y_3	0.499 ± 0.011	25	$[\frac{1}{\sqrt{2}}(Y-Z)]^{\otimes 4}$	-0.323 ± 0.012
12	Y_2Y_4	0.508 ± 0.011	26	$[\frac{1}{\sqrt{2}}(X+Y)]^{\otimes 4}$	0.645 ± 0.010
13	Y_3Y_4	0.560 ± 0.011	27	$[\frac{1}{\sqrt{2}}(X-Y)]^{\otimes 4}$	0.627 ± 0.010
14	$Y_1Y_2Y_3Y_4$	0.643 ± 0.010	W_{proj}		-0.099 ± 0.003
$F_{\text{D}_4^{(2)}}$		0.766 ± 0.003	W_5		-0.0132 ± 0.0005

TABLE XXXII. Results of fidelity and witness of four-photon Dicke state at noise $\theta = 2\pi/15$. Including the required 27 operator expectation values. Under the conditions of no filtering of the parametric light, pump laser power of 3100mw, PPKTP crystal temperature of 70℃. Data are collected for each basis in 60 s (about 5600 events). Error bars are derived from raw data analysis incorporating Poissonian counting statistics.

Operators		Expectation value	Operators		Expectation value
1	X_1X_2	0.586 ± 0.010	15	Z_1Z_2	-0.351 ± 0.012
2	X_1X_3	0.491 ± 0.011	16	Z_1Z_3	-0.332 ± 0.012
3	X_1X_4	0.512 ± 0.011	17	Z_1Z_4	-0.273 ± 0.012
4	X_2X_3	0.508 ± 0.011	18	Z_2Z_3	-0.274 ± 0.012
5	X_2X_4	0.521 ± 0.011	19	Z_2Z_4	-0.331 ± 0.012
6	X_3X_4	0.579 ± 0.010	20	Z_3Z_4	-0.338 ± 0.012
7	$X_1X_2X_3X_4$	0.645 ± 0.010	21	$Z_1Z_2Z_3Z_4$	0.901 ± 0.005
8	Y_1Y_2	0.419 ± 0.012	22	$[\frac{1}{\sqrt{2}}(X+Z)]^{\otimes 4}$	-0.338 ± 0.012
9	Y_1Y_3	0.364 ± 0.012	23	$[\frac{1}{\sqrt{2}}(X-Z)]^{\otimes 4}$	-0.348 ± 0.012
10	Y_1Y_4	0.384 ± 0.012	24	$[\frac{1}{\sqrt{2}}(Y+Z)]^{\otimes 4}$	-0.154 ± 0.013
11	Y_2Y_3	0.401 ± 0.012	25	$[\frac{1}{\sqrt{2}}(Y-Z)]^{\otimes 4}$	-0.241 ± 0.012
12	Y_2Y_4	0.408 ± 0.012	26	$[\frac{1}{\sqrt{2}}(X+Y)]^{\otimes 4}$	0.353 ± 0.012
13	Y_3Y_4	0.417 ± 0.012	27	$[\frac{1}{\sqrt{2}}(X-Y)]^{\otimes 4}$	0.361 ± 0.012
14	$Y_1Y_2Y_3Y_4$	0.115 ± 0.013	W_{proj}		0.017 ± 0.003
$F_{\text{D}_4^{(2)}}$		0.650 ± 0.003	W_5		-0.0085 ± 0.0005

[1] R. Raussendorf, D. E. Browne, and H. J. Briegel, Phys. Rev. A **68**, 022312 (2003).
[2] M. V. Larsen, X. Guo, C. R. Breum, J. S. Neergaard-Nielsen, and U. L. Andersen, Nat. Phys. **17**, 1018 (2021).
[3] Q. Zhao, Y. Zhou, and A. M. Childs, Nat. Phys. , 1 (2025).
[4] A. Karlsson and M. Bourennane, Phys. Rev. A **58**, 4394 (1998).
[5] J. Yin, Y.-H. Li, S.-K. Liao, M. Yang, Y. Cao, L. Zhang, J.-G. Ren, W.-Q. Cai, W.-Y. Liu, S.-L. Li, *et al.*, Nature **582**, 501 (2020).
[6] M. Proietti, J. Ho, F. Grasselli, P. Barrow, M. Malik, and A. Fedrizzi, Sci. Adv. **7**, eabe0395 (2021).
[7] A. W. Chin, S. F. Huelga, and M. B. Plenio, Phys. Rev. Lett. **109**, 233601 (2012).
[8] R. Demkowicz-Dobrzański and L. Maccone, Phys. Rev. Lett. **113**, 250801 (2014).
[9] L. Pezze, A. Smerzi, M. K. Oberthaler, R. Schmied, and P. Treutlein, Rev. Mod. Phys **90**, 035005 (2018).
[10] S. Cao, B. Wu, F. Chen, M. Gong, Y. Wu, Y. Ye, C. Zha, H. Qian, C. Ying, S. Guo, *et al.*, Nature **619**, 738 (2023).
[11] T. Jiang, J. Cai, J. Huang, N. Zhou, Y. Zhang, J. Bei, G. Cai, S. Cao, F. Chen, J. Chen, *et al.*, arXiv:2505.01978 (2025).
[12] M. Eibl, N. Kiesel, M. Bourennane, C. Kurtsiefer, and H. Weinfurter, Phys. Rev. Lett. **92**, 077901 (2004).
[13] G. Tóth, Phys. Rev. A **71**, 010301 (2005).
[14] G. Tóth and O. Gühne, Phys. Rev. Lett. **94**, 060501 (2005).
[15] N. Kiesel, C. Schmid, U. Weber, G. Tóth, O. Gühne, R. Ursin, and H. Weinfurter, Phys. Rev. Lett. **95**, 210502 (2005).
[16] N. Kiesel, C. Schmid, G. Tóth, E. Solano, and H. Weinfurter, Phys. Rev. Lett. **98**, 063604 (2007).
[17] C.-Y. Lu, X.-Q. Zhou, O. Gühne, W.-B. Gao, J. Zhang, Z.-S. Yuan, A. Goebel, T. Yang, and J.-W. Pan, Nat. Phys. **3**, 91 (2007).
[18] W. Wieczorek, R. Krischek, N. Kiesel, P. Michelberger, G. Tóth, and H. Weinfurter, Phys. Rev. Lett. **103**, 020504 (2009).
[19] R. Prevedel, G. Cronenberg, M. S. Tame, M. Paternostro, P. Walther, M. S. Kim, and A. Zeilinger, Phys. Rev. Lett. **103**, 020503 (2009).
[20] M. Seevinck and J. Uffink, Phys. Rev. A **76**, 042105 (2007).
[21] D. Rosset, R. Ferretti-Schöbitz, J.-D. Bancal, N. Gisin, and Y.-C. Liang, Phys. Rev. A **86**, 062325 (2012).
[22] S. Morelli, H. Yamasaki, M. Huber, and A. Tavakoli, Phys. Rev. Lett. **128**, 250501 (2022).
[23] H. Cao, S. Morelli, L. A. Rozema, C. Zhang, A. Tavakoli, and P. Walther, Phys. Rev. Lett. **133**, 150201 (2024).
[24] G. Tóth, C. Knapp, O. Gühne, and H. J. Briegel, Phys. Rev. Lett. **99**, 250405 (2007).
[25] G. Tóth, C. Knapp, O. Gühne, and H. J. Briegel, Phys. Rev. A **79**, 042334 (2009).
[26] O. Gittsovich, P. Hyllus, and O. Gühne, Phys. Rev. A **82**, 032306 (2010).
[27] Y.-C. Liang, D. Rosset, J.-D. Bancal, G. Pütz, T. J. Barnea, and N. Gisin, Phys. Rev. Lett. **114**, 190401 (2015).
[28] N. Miklin, T. Moroder, and O. Gühne, Phys. Rev. A **93**, 020104 (2016).
[29] M. Paraschiv, N. Miklin, T. Moroder, and O. Gühne, Phys. Rev. A **98**, 062102 (2018).
[30] I. Frérot and T. Roscilde, Phys. Rev. Lett. **127**, 040401 (2021).
[31] Z. Chen, F. Shi, and Q. Zhao, New J. Phys. **27**, 094503 (2025).
[32] M. Navascués, F. Baccari, and A. Acín, Quantum **5**, 589 (2021).
[33] G. N. M. Tabia, K.-S. Chen, C.-Y. Hsieh, Y.-C. Yin, and Y.-C. Liang, npj Quantum Inf. **8**, 98 (2022).
[34] F. Shi, L. Chen, G. Chiribella, and Q. Zhao, Phys. Rev. Lett. **134**, 050201 (2025).
[35] O. Gühne and G. Tóth, Phys. Rep. **474**, 1 (2009).
[36] G. Tóth, W. Wieczorek, R. Krischek, N. Kiesel, P. Michelberger, and H. Weinfurter, New J. Phys. **11**, 083002 (2009).
[37] N. Kiesel, C. Schmid, G. Tóth, E. Solano, and H. Weinfurter, Phys. Rev. Lett. **98**, 063604 (2007).
[38] G. Tóth, W. Wieczorek, D. Gross, R. Krischek, C. Schwemmer, and H. Weinfurter, Phys. Rev. Lett. **105**, 250403 (2010).
[39] T. Moroder, P. Hyllus, G. Tóth, C. Schwemmer, A. Niggebaum, S. Gaile, O. Gühne, and H. Weinfurter, New J. Phys. **14**, 105001 (2012).
[40] Y.-C. Liu, X.-D. Yu, J. Shang, H. Zhu, and X. Zhang, Phys. Rev. Appl. **12**, 044020 (2019).
[41] C. Schwemmer, G. Tóth, A. Niggebaum, T. Moroder, D. Gross, O. Gühne, and H. Weinfurter, Phys. Rev. Lett. **113**, 040503 (2014).
[42] T. Tashima, S. K. Ozdemir, T. Yamamoto, M. Koashi, and N. Imoto, J. Phys. Soc. Jpn. (2008).
[43] D. Wu, Q. Zhao, X.-M. Gu, H.-S. Zhong, Y. Zhou, L.-C. Peng, J. Qin, Y.-H. Luo, K. Chen, L. Li, N.-L. Liu, C.-Y. Lu, and J.-W. Pan, Phys. Rev. Lett. **127**, 230503 (2021).
[44] A. Chiuri, L. Mazzola, M. Paternostro, and P. Mataloni, New J. Phys. **14**, 217 (2012).
[45] Y. Y. Zhao, Y. C. Wu, G. Y. Xiang, C. F. Li, and G. C. Guo, Opt. Express **23**, 30491 (2015).
[46] L. Chen, L. Lu, L. Xia, Y. Lu, S. Zhu, and X. S. Ma, Phys. Rev. Lett. **130**, 7 (2023).
[47] B. P. Lanyon and N. K. Langford, New J. Phys. **11**, 1 (2008).
[48] B. Fang, M. Menotti, M. Liscidini, J. E. Sipe, and V. O. Lorenz, Phys. Rev. Lett. **123**, 070508 (2019).
[49] Z.-D. Li, X. Yuan, X.-F. Yin, L.-Z. Liu, R. Zhang, Y.-Y. Fei, L. Li, N.-L. Liu, X. Ma, H. Lu, Y.-A. Chen, and J.-W. Pan, Phys. Rev. Res. **2**, 023047 (2020).
[50] S. Kumar, D. Bhatti, A. E. Jones, and S. Barz, New J. Phys. **25**, 063027 (2023).
[51] N. Kiesel, C. Schmid, U. Weber, G. Tóth, O. Gühne, R. Ursin, and H. Weinfurter, Phys. Rev. Lett. **95**, 210502 (2005).
[52] Y. Tokunaga, S. Kuwashiro, T. Yamamoto, M. Koashi, and N. Imoto, Phys. Rev. Lett. **100**, 210501 (2008).
[53] C. Zhang, Y. F. Huang, B. H. Liu, C. F. Li, and G. C. Guo, Phys. Rev. A **93**, 062329 (2016).
[54] B. Jungnitsch, T. Moroder, and O. Gühne, Phys. Rev. Lett. **106**, 190502 (2011).
[55] M. Bourennane, M. Eibl, C. Kurtsiefer, S. Gaertner, H. Weinfurter, O. Gühne, P. Hyllus, D. Bruß, M. Lewen-

stein, and A. Sanpera, Phys. Rev. Lett. **92**, 087902 (2004).
[56] O. Gühne and P. Hyllus, Int. J. Theor. Phys. **42**, 1001 (2003).
[57] O. Gühne, C.-Y. Lu, W.-B. Gao, and J.-W. Pan, Phys. Rev. A **76**, 030305 (2007).
[58] Y. Tokunaga, T. Yamamoto, M. Koashi, and N. Imoto, Phys. Rev. A **74**, 020301 (2006).
[59] D. F. V. James, P. G. Kwiat, W. J. Munro, and A. G. White, Phys. Rev. A **64**, 052312 (2001).
[60] C. K. Hong, Z. Y. Ou, and L. Mandel, Phys. Rev. Lett. **59**, 2044 (1987).